ROMANIA

MINISTRY OF NATIONAL DEFENSE

MILITARY TECHNICAL ACADEMY „FERDINAND I”

FACULTY OF COMMUNICATIONS AND ELECTRONIC SYSTEMS FOR DEFENSE AND SECURITY

MASTER PROGRAM: COMMUNICATION SYSTEMS ENGINEERING AND ELECTRONIC SECURITY

# ”THE ANALYSIS OF SIGNALS FROM ULTRA-WIDEBAND SYSTEMS”

# ”ANALIZA SEMNALELOR PROVENITE DIN SISTEME UWB”

Coordinating professor:

Cpt. conf. univ. dr. ing. Angela DIGULESCU-POPESCU

Master student:

Slt.ing. Paraschiva-Cristina POPOVICI



Bucharest 2022

6 din

Declaraţie pe propria răspundere privind originalitatea lucrării de disertaţie

Subsemnata Popovici Paraschiva-Cristina, domiciliată în comuna Botoșana, judeţul Suceava, legitimată cu CI, seria XV, Nr. 113055, CNP 2971221330241, declar pe proprie răspundere şi în conformitate cu art. 292 Cod Penal, privind falsul în declaraţii, că lucrarea cu titlul: „The analysis of signals from Ultra-wideband systems", în limba română "Analiza semnalelor provenite din sisteme UWB", elaborată în vederea susţinerii examenului de finalizare a studiilor de masterat, organizat de către Facultatea de Comunicații și sisteme electronice pentru apărare și securitate din cadrul Academiei Tehnice Militare "Ferdinand I", sesiunea iunie a anului universitar 2021-2022, având conducător de lucrare pe cpt. conf. univ. dr. ing. DIGULESCU-POPESCU Angela-Manuela, reprezintă o contribuţie proprie, originală.

La realizarea lucrării am folosit doar sursele bibliografice menţionate în subsolul paginilor şi în bibliografia prezentată la sfârşitul lucrării, cu respectarea legislaţiei române şi a convenţiilor internaţionale privind drepturile de autor.

Lucrarea este elaborată de mine şi nu reprezintă un plagiat, nu a mai fost prezentată în cadrul vreunei instituții de învățământ superior din țară sau străinătate în vederea obținerii unui grad sau titlu didactic ori științific.

Data Semnătură:

Profesor coordonator:

Cpt. conf. dr. ing. DIGULESCU-POPESCU Angela-Manuela

Absolvent:

Slt.ing. Paraschiva-Cristina POPOVICI

# Abstract

Ultra-wideband (UWB) signals are signals of duration of nanoseconds in time domain, occupying a very large frequency bandwidth of GHz order. UWB is used for surveillance, detection, positioning and other applications due to its fine temporal resolution and low emission power. This paper presents some signal processing methods for UWB signal such as Envelope Detection via Hilbert Transform, Power Spectral Density Estimation via Welch's method, Baseband Conversion, Matched Filter and Search Subtract and Readjust algorithm. People detection and counting using an IR-UWB based on Artificial Intelligence algorithms is presented as application in the second part of this paper. Three approaches for feature extraction are proposed, first based on a complex hybrid feature extraction method consisting of the Curvelet Transform method and a segmented-based feature extraction method, the second by using a Convolutional Neural Network (CNN) on the raw dataset and third by using Principal Component Analysis (PCA) algorithm for data compressing both for the raw dataset and the set of hybrid features. The classification is done by using AI algorithms such as K-nearest neighbours (KNN), Support Vector Machine (SVM), Multilayer Perceptron Neural Network (MLP) and Convolutional Neural Network. The algorithms' performance is provided in terms of accuracy, precision, recall and f1-score functions. The results show great performance for MLP using the hybrid features (the frequency-based and time-based features), where the accuracy is 99.85%. The drawback would be the high computational demand, so CNN applied on the set of features resulted from applying PCA on the entire dataset is recommended for real-time applications, which shows an accuracy of 95.41%. Data compression provided by PCA provides fast training and testing, but the data insufficiency can degrade the performance, if not a large dataset is used.

10 din

# Table of Contents

# List of figures

## List of tables

# Rezumat

Această lucrare se referă la tehnologia ultra-wideband (UWB) și este împărțită în patru capitole : Capitolul 1 Introducere în tehnologia ultra-wideband, Capitolul 2 Metode de procesare de semnal pentru semnale UWB, Capitolul 3 Detecția și numărarea de persoane folosind un radar IR-UWB bazate pe algoritmi de inteligență artificială și Capitolul 4 Rezultate și concluzii, iar lucrarea se finalizează cu referințe bibliografice.

Primul capitol face o introducere în concept de bază pentru tehnologia UWB. Standardul IEEE 802.15.4 vizează tehnologia Ultra-wideband, o tehnologie ce permite comunicații de putere și cost scăzut, folosită în rețele wireless personale (WPAN). Standardul IEEE 802.15.4 este descris în RFC 8137 [1] și alte documente similare și se referă la nivelul fizic și nivelul MAC (Medium Access Control) folosite de protocolul UWB, protocoale IoT precum ZigBEE sau WirelessHART, etc. Protocolul UWB s-a dezvoltat în ultimii 20 de ani pentru aplicații de supraveghere și securitate, comunicații radar, localizare indoor, aplicații radar through-the-wall, datorită avantajului de a permite comunicații de date cu viteză de transfer foarte mare (Mbps/ Gbps) și a lățimii de bandă foarte mare (> 500 MHz), ceea ce oferă rezoluție temporală foarte bună [2].

Semnalele UWB sunt semnale cu o durată de ordinul nanosecundelor în domeniul timp, care ocupă o bandă de cel puțin 500 MHz în domeniul frecvență. Banda de frecvențe nelicențiată alocată pentru acest protocol se află în intervalul 3.1 GHz – 10.6 GHz, ocupând în total 7.5 GHz [3]. Un dispozitiv e cosiderat a fi de bandă foarte largă dacă are banda fracțională de -10 dB, sau mai mult de 20% din frecvența centrală [4]. Banda foarte largă face această tehnologie potrivită pentru aplicații de localizare și urmărire, datorită rezoluției temporale foarte bune.

Pentru anumite regiuni geografice (Europa, SUA, Japonia, Canada) Federal Communications Commission impune anumite condiții pentru tehnologia UWB în ceea ce privește puterea spectrală de emisie și lățimea de bandă. Pentru Europa, limitările măștii privind puterea spectrală de emisie este sub -43 dBm/MHz. Unul

dintre avantajele acestui protocol este costul redus de putere de emisie < 0.5 mW, ceea ce face ca interferențele cu alte dispozitive de bandă îngustă să nu aibă loc, și care îi dă posibilitatea semnalului de a nu fi interceptat, fiind robust la zgomot și propagare multicale severă sau bruiaj [5].

Comunicația UWB este influențată de răspunsul la impuls al canalului de propagare, care poate să cauzeze propagarea multicale [6]. Interacțiunea cu obiectele care se află între emițător și receptor cauzează fenomene precum reflexii, refracții, difracții și absorții, ceea ce conduce la propagarea multicale, unde la recepție semnalul este suma unor versiuni întârziate și atenuate ale semnalului original transmis. Pentru sistemele de bandă foarte largă, atenuarea spațiului liber, efectul difracțiilor și reflexiilor sunt dependente de frecvență [7].

Canalul de propagare afectează diferit semnalele UWB, în comparație cu semnalele de bandă îngustă, din cauza lățimii de bandă. Câștigul în amplitudine a semnalelor recepționate este dependent de frecvență, la fel și timpii de întârziere a semnalelor reflectate de mediu. Estimarea canalului este importantă în aplicații precum detecție de obiecte sau persoane, localizare și urmărire indoor, de asemenea diferențierea condițiilor de propagare (LOS/NLOS – condiții de vizibilitate directă/nevizibilitate directă) servește în aplicații precum comunicație vehicul-la-vehicul [7]. Câștigul în amplitudine descrie atenuarea medie a semnalului transmis între emițător și receptor, care depinde și de distanța dintre acestea. Numărul de componente multicale (MPC) care pot apărea într-un cluster depinde de mediul de propagare, mai multe obiecte și un exces de întârziere pot determina apariția unui număr mai mare de MPCs, însă o lățime de bandă mai largă reduce numărul de MPCs [6]. Creșterea întârzierii determină creșterea fading-ului. Răspunsul la impuls al canalului acționează ca un filtru asupra semnalului emis, astfel condițiile de propagare de nevizibilitate direct determină un efect mai mare asupra semnalelor emise, de aceea e nevoie ca semnalele să fie preprocesate la recepție, pentru înlăturarea zgomotului și pentru extragerea componentelor multicale.

Capitolul al doilea propune niște metode de procesare de semnal pentru semnale UWB, cum ar fi Detecția de anvelopă folosind Transformata Hilbert,

Estimarea Densității Spectrale de Putere folosind Metoda Welch, Conversia în banda de bază a semnalelor UWB, Filtrul adaptat la semnalul UWB și algoritmul Search Subtract and Readjust pentru extragerea componentelor multicale.

Detecția de anvelopă folosind Transformata Hilbert se folosește în aplicații de clasificare de imagini, aplicații de poziționare, determinarea perioadei semnalului, etc. Pentru a determina anvelopa unui semnal se folosește valoarea absolută a semnalului analitic, care este compus din suma semnalului original și transformata sa Hilbert.

Estimarea Densității Spectrale de Putere (PSD) folosind Metoda lui Welch presupune segmentarea suprapusă a unei serii de timp și înmulțirea segmentelor cu o funcție fereastră și ulterior efectuarea Transformatei Fourier Discrete asupra rezultatului înmulțirii. Banda utilă a unui semnal se poate determina prin aplicarea unui prag impus asupra PSD rezultate. Funcțiile fereastră folosite sunt Fereastră Rectangulară, Barlett, Hanning, Hamming sau Blackman.

Conversia în banda de bază presupune multiplicarea semnalului cu un semnal de referință care are aceeași frecvență centrală și ulterior filtrarea acestuia cu un filtru trece jos, având o frecvență de tăiere egală cu diferența dintre frecvența superioară a semnalului inițial și frecvența centrală.

Filtrul adaptat la semnalul UWB este proiectat astfel încât să maximizeze raportul semnal pe zgomot al semnalului de intrare. Acesta presupune convolutarea semnalului inițial cu un semnal de referință, care este semnalul inițial inversat în domeniul timp.

Algoritmul Search Subtract and Readjust este folosit pentru a detecta componentele multicale din semnalul recepționat. Amplitudinea și întârzierea componentelor sunt iterativ estimate, bazate pe extracția primei componente găsite în semnal, rezultând în semnalul rezidual. Raportul semnal pe zgomot al semnalului rezidual este iterativ maximizat prin folosirea filtrului adaptat la semnal. Parametrii celei mai puternice componentei multicale, adică amplitudinea și timpul de sosire, sunt estimați din valoarea absolută a rezultatului aplicării filtrului adaptat. Validarea algoritmului s-a realizat pe baza semnalelor sintetice,

unde răspunsul la impuls al canalului a fost dat ca referință, considerându-se cinci componente multicale. Forma de undă folosită corespunde a derivatei a doua Gaussiene. Pentru calcularea valorii bias și variației parametrilor estimați s-au realizat un număr de 1000 de simulări Monte Carlo, adică un număr de 1000 de semnale afectate de zgomot Gaussian cu valori ale raportului semnal pe zgomot între -10 și 0 dB. S-a constatat că amplitudinile estimate urmează o distribuție normală, fiind direct afectate de SNR, iar întârzierile estimate urmează o distribuție uniformă. Distribuțiile sunt validate de testul statistic Kolmogorov-Smirnov. Performanța estimatorului SSR este redat folosind Borna Cramer-Rao, unde raportul variațelor este aproximativ egal cu 1.

Capitolul trei descrie o aplicația de detecția și numărare de persoane folosind un radar IR-UWB bazat pe algoritmi de inteligență artificială precum K-nearest neighbours (KNN), Support Vector Machine (SVM), Multilayer Perceptron Neural Network (MLP) și Convolutional Neural Network (CNN).

Detecția, numărarea, localizarea și urmărirea de persoane este utilă în aplicații ce vizează securitatea și supravegherea unui mediu, de exemplu industrial sau medical, pentru supravegherea persoanelor aflate în dificultate, pentru detecția persoanelor aflate sub dărâmături, în cazul unui dezastru, pentru detecția persoanelor aflate într-o mașină, etc. Metodele tradiționale propun folosirea camerelor de supraveghere sau a senzorilor lidar, însă intervin probleme de invadare a informațiilor cu caracter personal, în cazul camerelor de supraveghere, și o perfomanță scăzută în cazul senzorilor lidar, dacă condițiile mediului sunt neoptime (fum, ceață, ploaie).

Radarul Impuls Radio Ultra-wideband (IR-UWB) este o alternativă eficientă, care depășește problemele celorlalte metode, furnizând o rezoluție temporală foarte bună, având un cost redus de putere. Radarele Impuls Radio Ultra-wideband (IR-UWB) transmit serii de impulsuri de durată și putere foarte mică, care sunt reflectate de mediu, semnal ulterior recepționat de receptor, după parcurgerea unei distanțe dus-întors. Caracteristicile țintei sunt redate de proprietățile semnalului ecou [8].

În literatura de specialitate există mai multe abordări pentru detectarea și numărarea de persoane folosind un radar IR-UWB. Metodele convenționale de detecție presupun compararea puterii semnalului recepționat cu un prag fix sau adaptiv [9] . Dezavantajul acestor metode este o rată înaltă de alarmă falsă din cauza surselor de zgomot și a fluctuației suprafeței efective de reflexe a țintei, care pot degrada performanțele detecției [9]. Din aceste motive, semnalul recepționat necesită a fi prelucrat, pentru înlăturarea zgomotului și a clutter-ului. Metodele folosite în literatură sunt: Exponential Average, Singular Value Decomposition, Filtrul Kalman, algoritmul CLEAN care presupune cross-corelația unui semnal șablon cu semnalul recepționat și extragerea acestuia [10], de asemenea o variantă îmbunătățită a algoritmului CLEAN se propune în articolul [11], pentru extragerea caracteristicilor pentru numărarea de persoane în medii dense. O altă metodă pentru detecția oarbă folosind un radar UWB, adică fără a avea cunoștință a priori de caracteristicile semnalului, este propusă în [12], și se bazează pe analiza seriilor de timp folosind Cross Recurrence Plot.

Detecția umană folosind un radar UWB se realizează analizând semnături micro-Doppler, articolul [8] se folosește de analiza acestor semnături pentru a pentru a evidenția mersul uman. Efectul Doppler apare atunci când semnalul transmis de radar lovește o țintă în mișcare, așadar frecvența purtătoare se modifică, viteza cu care aceasta se mișcă putând fi determinată. Semnăturile micro-Doppler se referă la vibrații și rotații ale țintei.

Pentru o mai bună acuratețe a detecției, numărării, localizării și urmăririi umane, s-au dezvoltat noi metode bazate pe algoritmi de Machine Learning și Deep Learning, majoritatea având ca date de intrare fie spectrogramele semnalelor recepționate sau semnături Doppler și micro-Doppler, unde algoritmi precum Rețele Neurale Profunde [9] [13], Rețetele Neurale Convoluționale [14] [15] sau Support Vector Machine [16] [17] sunt folosiți pentru clasificare.

În cazul de față, pentru clasificarea numărului de persoane se presupun trei metode, iar baza de data folosită corespunde referinței [18], unde se presupun patru scenarii. Primul scenariu se referă la un număr de persoane de la 0 la 10 care se plimbă aleator într-o încăpere, al doilea scenariu presupune de la 0 la 15 persoane

care stau la o coadă, cu o medie de 10 cm distanță între persoane, al treilea scenariu presupune de la 11 la 20 de persoane care se plimbă aleator în raza de acoperire a radarului, cu o densitate de trei persoane pe metru pătrat, iar ultimul scenariu se referă la un număr de la 11 la 20 de persoane care se plimbă aleator în raza de acoperire a radarului, cu o densitate de patru persoane pe metru pătrat.

Prima metodă implică extragerea unui set de caracteristici hibride, format din caracteristici de frecvență și caracteristici de timp. Caracteristicile de frecvență se referă la coeficienții curvelet, unde Transformata Curvelet presupune folosirea Transformatei Discrete Rapide Curvelet, folosind metoda wrapping [19]. Caracteristici de energie și amplitudine sunt extrase din stratul de tip coarse, detail și fine, care corespund frecvențelor joase, medii și înalte. Metoda de extragere a caracteristicilor bazate pe timp este metoda bazată pe segmentarea semnalului în segmente de dimensiune 32, 64 și 128 eșantioane, corespunzând distanței de 125, 250 și 500 mm în eșantionul radar. În total se extrag 280 caracteristici dintr-un eșantion radar cu dimensiunea de 50x1280 eșantioane. Clasificarea se realizează cu ajutorul metodelor KNN, SVM și MLP, cu mențiunea că setul de etichete este format din numărul de persoane și numărul scenariului.

A doua metodă presupune aplicarea unei Rețele Neurale Convoluționale asupra setului inițial de date, unde ca date de intrare se folosesc tensori de dimensiunea 1x50x1280, corespunzător eșantionului radar.

A treia metodă se referă la compresia datelor cu ajutorul Analizei în Componente Principale. PCA este aplicat pe setul inițial de date, de unde se extrag 6 componente principale, folosite ca date de intrare pentru o Rețea Neuronală Convoluțională, dar de asemenea aplicat asupra setului de caracteristici hibride, de unde se extrag 3 componente principale, folosite ca date de intrare pentru KNN, SVM și MLP. Pentru CNN se specifică că pentru setul de etichete se consideră doar numărul de persoane, nu și scenariul.

Validarea modelelor se realizează cu ajutorul metricilor de clasificare precum acuratețe, precizie, recall și f1-score.

Capitolul patru prezintă partea practică cu rezultate și concluzii. Pentru metodele de procesare de semnal propuse, se achiziționează un set de semnale UWB, unde sistemul de emisie este realizat din două generetoare de semnal: un generator de undă arbitrară, care generează semnalul ideal UWB în banda de bază, cu o durată a pulsului de 5 ns, ocupând o bandă de 2 GHz. Ulterior, semnalul este translatat pe o frecvență centrală de 7.25 GHz cu ajutorul unui generator radio-frecvență. Semnalul rezultat este un semnal cu o perioadă de 90ns. Sistemul de emisie reprezintă un osciloscop care funcționează la o rată de eșantionare de 40GHz. Semnalele sunt emise prin cablu și wireless. Metodele propuse în capitolul doi sunt aplicate semnalelor recepționate, cărora li se extrage componenta de curent continuu, se determină perioada semnalului cu ajutorul detecției de anvelopă, se determină banda semnalului cu ajutorul aplicării unu prag asupra PSD, se filtrează trece bandă în banda determinată, se convertesc în banda de bază prin convolutarea cu un semnal de referință având aceeași frecvență centrală, și se aplică algoritmul SSR care presupune și folosirea filtrului adaptat la semnal, unde semnalul ideal inițial transmis se folosește ca referintă. În urma aplicării algoritmului SSR se extrag trei componente multicale, care prezintă un fading lent, și se observă că prima componentă nu are neapărat cea mai mare amplitudine.

În ceea ce privește aplicația propusă de numărare de persoane, se observă cea mai mare performanță este dată de către MLP aplicat asupra setului de caracteristici hibride, unde acuratețea este de 99.85%, urmat de KNN cu 94.08%. De asemenea, se observă că CNN aplicat setului de date compus din componentele principale extrase cu ajutorul PCA prezintă o performanță destul de bună, cu o acurateţe de 95.41%, drept pentru care este recomdantă în aplicații în timp real, deoarece, vizavi de prima metodă care necesită o mai mare complexitate și un timp îndelungat de procesare a datelor, aceasta este eficientă din punct de vedere al resurselor de calcul.

Această lucrare pune în valoare eficiența algoritmilor de inteligență artificială propuși și a tehnologiei ultra-wideband, care prezintă avantajele specificate mai sus. De asemenea, se observă că în funcție de context, trebuie să se facă un compromis între performanță, rapiditate și eficiență computațională.

# Chapter 1

## 1.1 Introduction

Surveillance, safety and security are important aspects of human-machine interaction in hospitals [20], perceptive car scenarios, smart factories, and so on. Detection and localization techniques, such as computer vision, infrared detectors, LADAR (Laser Detection and Ranging) signatures, UWB radar [21], Global Positioning System (GPS), vibration and seismic sensors, and acoustic sensors [20] were recently developed for ensuring human safety by detection and localization of moving persons or objects, and not only.

In the last 20 years, UWB technology has been developed for high data rate communications, radar communications, surveillance and safety applications, indoor localization, through-wall radar applications and other niche applications. UWB is used in Personal Area Networks, having a short coverage area of approximately 10 meters [22].

Line of sight (LOS) [23] , bad weather conditions, environmental interference and privacy issues [24] could degrade and prevent the performance of enumerated technologies, except for UWB radar, which is appropriate for any kind of environment due to its high range resolution [21] and noise robustness.

## 1.2. UWB technology theoretical concepts

UWB technology is a wireless technology, used in WPAN (Wireless Personal Area Network) networks, introduced due to the need for higher data transfer speed (Mbps, Gbps) [2].

UWB signals are very short-term pulses (ns), occupying a wide spectrum. The unlicensed spectrum allocated for the ultra-wideband devices (UWB) is within the 3.1 GHz – 10.6 GHz frequency range, occupying the 7.5 GHz bandwidth [3]. A device is considered ultra-wideband if the fractional bandwidth is -10 dB or more than 20% of the central frequency [4]. Its large bandwidth makes this technology suitable for localization and tracking applications, providing high temporal resolution.

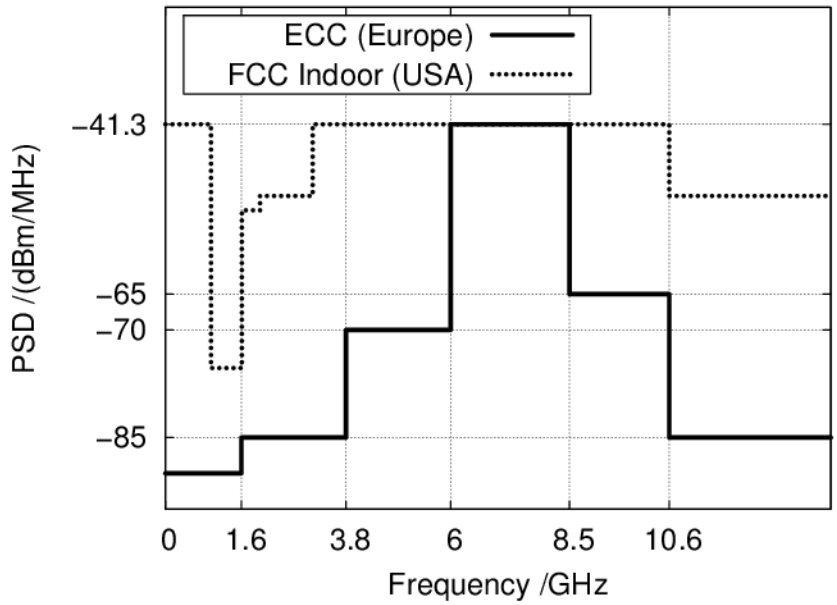


Figure 1 FCC and ECC mask limitations [25]

The Federal Communications Commission (FCC) and Electronic Communications Committee (ECC) mask limitations concerning transmission power limitations and allocated bandwidth. These limitations are imposed to avoid interference with other devices. In Romania, the regulatory regime for UWB technology is ECC Rec 70-03 /ECC Decision 06(04) / ETSI EN 302 065, which permits a frequency range of 3.1 – 4.8 GHz, 6.0 – 8.5 GHz and 8.5 – 9.0 GHz. The maximum equivalent isotropic radiated power (EIRP) is -41.3 dBm/ MHz [26].

One of the advantages of this technology is the low consumption of resources, using a very low emission power ($P_t$ < 0.5 mW). A signal that occupies a

very wideband and uses a very low transmission power is similar to noise in the time domain, being resistant to jamming, providing a low probability of interception and detection, and being advantageous for secret military applications [27].

An UWB radar can be used for security, rescue and surveillance applications [28], providing a good range resolution, which makes it a suitable technique for human movement detection [20].

An UWB radar transmits a series of short-term, low-power pulses [29], which are reflected by the environment, travel a round trip distance, later received by the radar receiver [30]. The radar echo signal is analyzed for human or object detection [29]. The characteristics of the target are given by the changes in the properties of the echo signal [31].

## 1.3 Channel estimation

The UWB communication is influenced by the propagation channel, causing multipath propagation [32]. Phenomena such as reflection, diffraction, and absorption are due to the interaction of the emitted pulse with different objects in the environment in which the system operates. Each interaction can cause direction changing and delays, and this leads to splitting up the components into new ones [33]. For UWB systems, due to their large bandwidth, the free-space attenuation, and the effect of diffraction, reflection at dielectric walls are frequency-dependent [34].

The multipath components have a delay, an attenuation and a direction of arrival, depending on the path they take. Differentiating the channel propagation conditions (LOS/NLOS) is important for applications such as indoor localization or vehicle-to-vehicle communication [35].

The propagation channel has a different effect on UWB signals in comparison to narrowband signals, due to their large bandwidth. The path gain of

the received signal is frequency-dependent, as well as the time delays of the clusters and rays. A cluster is a group of multipath components, due to the multipath propagation.

The main standard which describes the channel estimation is IEEE 802.15.4a. There are ten proposed channel models, based on the change of the specific parameters due to the environmental conditions and the other channel effects.

Table 1. IEEE 802.15.4a Channel models

| Channel Number | Environments | Propagation |
|---|---|---|
| CM1 | Indoor residential | LOS |
| CM2 | Indoor residential | NLOS |
| CM3 | Indoor office | LOS |
| CM4 | Indoor office | NLOS |
| CM5 | Outdoor | LOS |
| CM6 | Outdoor | NLOS |
| CM7 | Industrial | LOS |
| CM8 | Industrial | NLOS |
| CM9 | Open outdoor | NLOS |
| BAN | Body area network | NLOS |

The channel model proposed by IEEE 802.15a is derived from the Saleh-Valenzuela model which states that the received signal is composed of clusters and rays, each having independent fading, meaning attenuated and delayed versions of the transmitted signal. The arrival times of clusters and rays follow a Poisson distribution [36], where the multipath gain magnitude follows a log-normal distribution [22].

The received signal is considered as:

$$r(t) = \int_{-\infty}^{\infty} c(t,\tau)w(t-\tau)d\tau + n(t) \quad (1)$$

Where the terms represents:

$\tau$ : the delay

$n(t)$ : the additive Gaussian noise

$w(t-\tau)$ : the delayed version of the emitted signal

$c(t,\tau)$ : the channel impulse response which is a time-variant

The channel impulse response equation is given as follows:

$$c(t) = \sum_{c=1}^{C} \sum_{r=1}^{R_c} a_{cr} \delta(t - T_c - \tau_{cr}) \quad (2)$$

Where the terms represents:

$C$ : the number of clusters (groups of multipath rays arriving in the receiver)

$R_c$ : the number of multipath components of the cluster

$T_c$ : the arrival time of each cluster

$\tau_{cr}$ : the arrival time of each multipath component in the cluster

$\delta$ : Dirac delta function

$a_{cr}$ : the multipath gain coefficient

The path gain describes the average attenuation of the signal transmitted from the emitter Tx to the receiver Rx, which depends on the distance between the emitter and the receiver [33].

The number of multipath components which can occur within a cluster depends on the environment, more objects in the environment and a larger excess delay can determine more multipath components (MPCs), a large bandwidth

reduces the number of MPCs per delay bin [33]. The increasing delay determines the increase of fading.

Depending on the environment and propagation conditions, channel impulse response may affect the signal propagation differently, some examples of channel impulse response in the industrial environment with LOS and NLOS propagation and their energy-delay profiles are given in the images below:

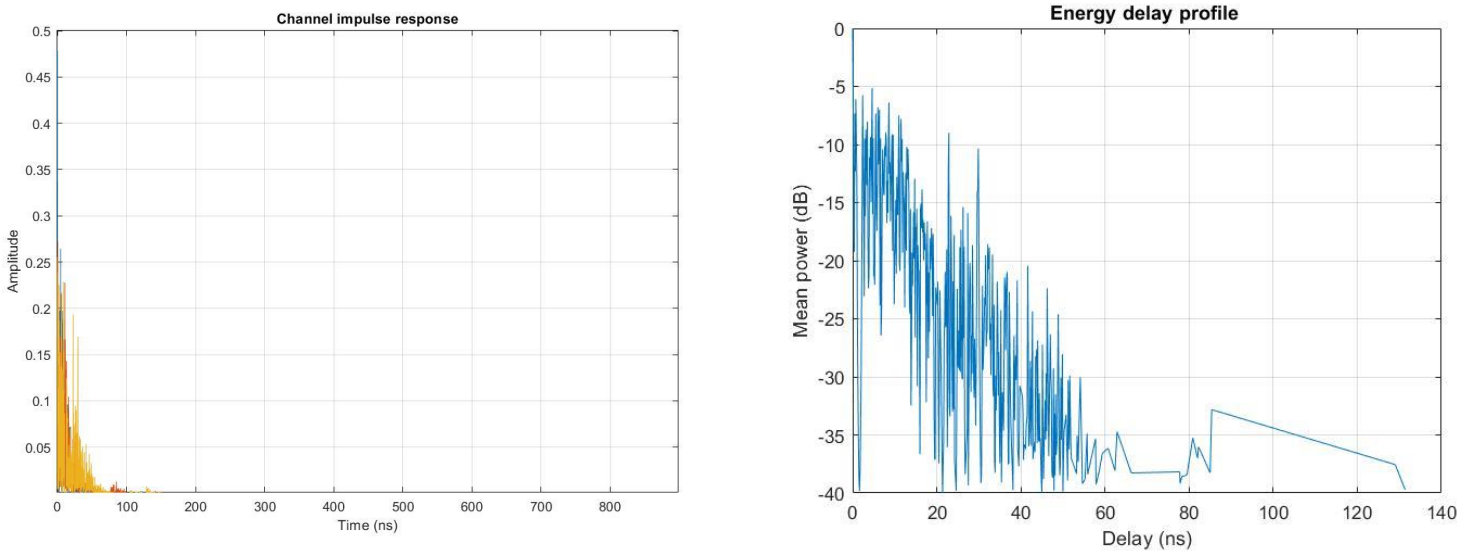


Figure 2 CM3 Indoor office (Line of Sight)

The channel impulse response acts as a filter upon the emitted signal, thus Non-Line of Sight propagation conditions determines a greater effect on the transmitted signals, phenomena such as reflections and diffraction are determined by the objects between the emitter and the receiver. Data need to be preprocessed at the receiver side to distinguish the desired signal from the clutter and noise.

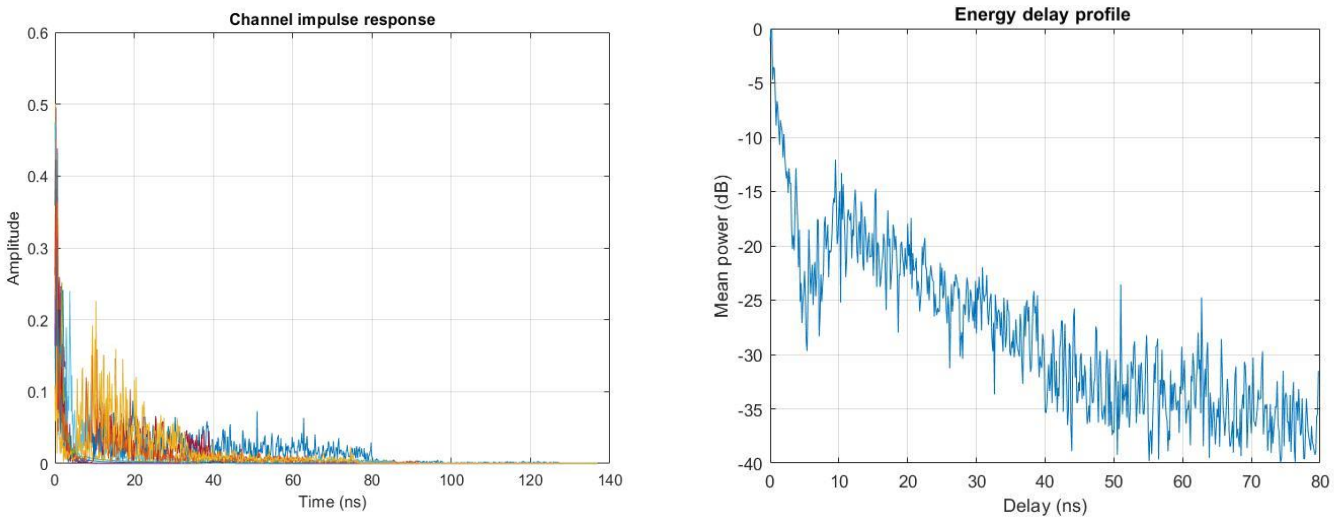


Figure 3. CM7 Industrial (Line of Sight)

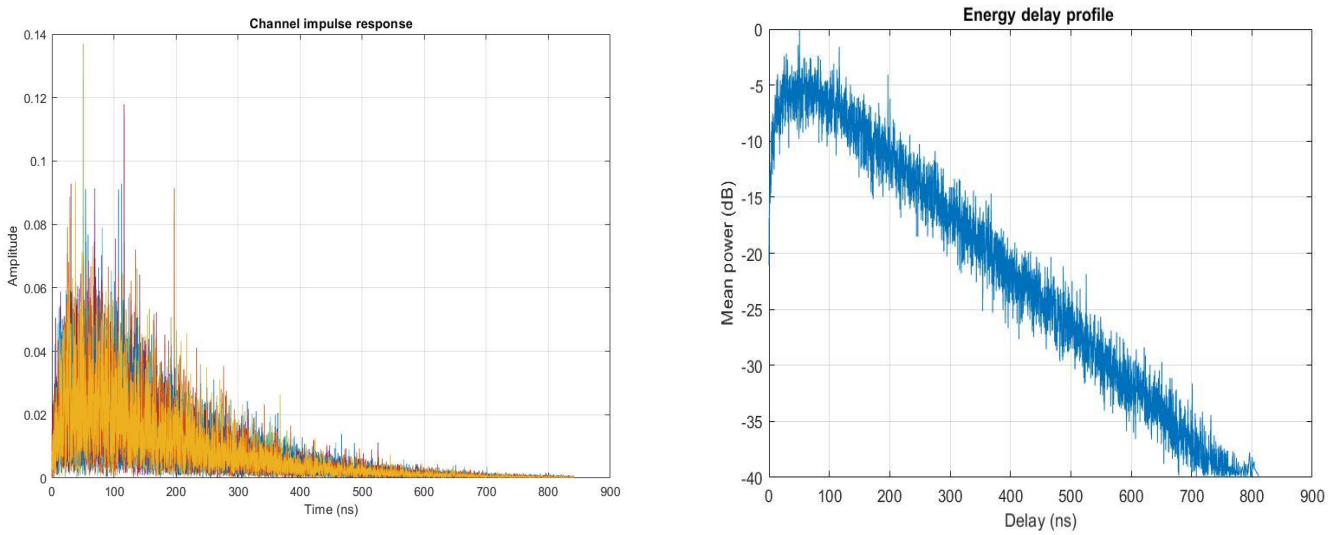


Figure 4 CM8 Industrial (Non-Line of Sight)

30 din

# Chapter 2

# UWB Signal Processing Methods

The objectives of this chapter are to present some signal processing techniques for UWB signals and channel estimation, such as envelope detection via Hilbert Transform for signal period estimation, Power Spectral Density Estimation via Welch Method for determining the signal bandwidth, Matched filter for the signal to noise ratio maximizing, Search Subtract and Readjust method for multipath components extraction.

## 2.1. Envelope Detection using Hilbert Transform

The signal envelope detection could have application in finding the period of a signal, in imagery classification, in application for positioning and others. To determine the envelope of the original waveform $g(t)$, the absolute value of the analytic signal is used [37]. The analytical signal is composed of the original signal and its Hilbert Transform and has no negative frequency components.

Given a signal $g(t)$, the absolute value of the analytic signal $G_a(t)$, which is composed of the original waveform $g(t)$ and its Hilbert transform $\tilde{g}(t)$, can be used to determine the signal's envelope:

$$G_a(t) = g(t) + i\tilde{g}(t) \tag{3}$$

The Hilbert Transform presumes that the original signal is filtered by a filter with an impulse response function of $h(t) = \frac{1}{\pi t}$.

$$\tilde{g}(t) = g(t) * \frac{1}{\pi t} \tag{4}$$

In the frequency domain, the expression of the Hilbert Transform of $g(t)$ will be as follows:

$$F\{\hat{g}(t)\} = [G_{-}(f) + G_{+}(f)]\big(-j\,\mathrm{sgn}(f)\big) = jG_{-}(f) - jG_{+}(f) \quad (5)$$

The analytic signal is constructed by suppressing all the negative frequency of the real signal and can be written as:

$$G_a(f) = G_{-}(f) + G_{+}(f) + j[jG_{-}(f) - jG_{+}(f)] \quad (6)$$

$$G_a(f) = 2\,G_{+}(f) \quad (7)$$

The envelope detection is performed using the absolute value of the analytical signal.

## 2.2 Power Spectral Density Estimation via Welch's method

"Power Spectral Density describes the power of a signal or time series distributed over different frequencies" [38] .

The Discrete Fourier Transform of the autocorrelation of a signal $x(t)$ is called the Power Spectral Density (PSD) [38], where $R_{xx}(k)$ is the autocorrelation function of the signal $x(t)$.

$$S_{xx}(f) = \sum_{k=-\infty}^{\infty} R_{xx}(k)e^{-i\omega kT} \quad (8)$$

Welch's method requires the segmentation of a time series of length N in L overlapped segments of length M, multiplied by an established window function, then computing DFT on each segment:

$$x_m(n) = w(n)x(n + mR) \quad (9)$$

Where:

$n = 0..M-1$ represents the window length

$m = 0,1,\ldots K-1$ the m′th windowed frame

R : window hop size

K : the available frames

Welch's estimate of Power Spectral Density is given as follows:

$$S_x^W(f) = \frac{1}{K}\sum_{m=0}^{K-1} P_{x_{m,M}}(f) \tag{10}$$

Where:

$$P_{x_{m,M}}(f) = \frac{1}{M}\left|\sum_{n=0}^{N-1} x_m(n)e^{-j2\pi nk/N}\right|^2 \tag{101}$$

The window function such as Rectangular window, Barlett window, Hanning window, Hamming window or Blackman window [38] are used for PSD estimation via Welch's method.

To determine the bandwidth of interest for the reference UWB signal, a PSD estimation via Welch's Method is computed, using a Hamming window function of an input signal period`s length, with 0 overlap samples for better noise reduction in the estimated power spectrum. The Hamming window function is the following:

$$W(n) = \begin{cases} 0.54 + 0.446\cos\left(\frac{2\pi n}{N}\right), |n| < \frac{N-1}{2} \\ 0, \text{otherwise} \end{cases} \tag{11}$$

## 2.3 Baseband Conversion

To convert a signal to the baseband requires the multiplication of the input signal with a reference signal having the same central frequency $f_c$, then a low pass filtration at the cutoff frequency $f_{cutoff}$ equal to the subtraction of the upper frequency and the central frequency.

$$f_c = f_{upper} - \frac{BW}{2} \quad (12)$$

$$f_{cutoff} = f_{upper} - f_c \quad (13)$$

Where

$f_{upper}$ : the upper frequency of the input signal

BW : the input signal's frequency bandwidth

## 2.4 Matched Filter

Matched filters are designed to maximize the signal to noise ratio (SNR) of an input signal. This is accomplished by the convolution of the signal with the template waveform, which is the time reverse input signal [39].

Given an input signal $(t) = x(t) + n(t)$ , where $x(t)$ is the signal of interest and $n(t)$ is the noise, the maximum SNR at the output will occur when the filter has an impulse response that is time-reverse of the input signal [39].

The convolution of this impulse response with the signal $x(t)$ provides the autocorrelation in the input signal. The matched filter is defined by an impulse response which corresponds to the reverse time reference signal, as:

$$h(t) = x(T - t) \tag{14}$$

where T is the period of the template signal.

## 2.5 Search Subtract and Readjust

The received UWB signal will be a sum of attenuated and delayed versions of the ideal reference emitted signal, due to the multipath propagation, according to the Saleh Valenzuela model. The propagation channel acts as a filter, so to estimate the multipath components, channel impulse response needs to be estimated.

A method for channel estimation and determination of Time of Arrival and the amplitudes of the multipath components is Search Subtract and Readjust method, proposed in [40].

Let $c(t)$ be the channel impulse response, with $c_l$ and $\tau_l$ the amplitudes and delays of the L multipath components [40]:

$$c(t) = \sum_{l=1}^{L} c_l \delta(t - \tau_l) \tag{15}$$

Let $w(t)$ be the ideal received pulse, $n(t)$ the additive Gaussian noise and $r(t)$ the received signal:

$$r(t) = \sum_{l=1}^{L} c_l w(t - \tau_l) + n(t) \tag{16}$$

The additive Gaussian noise has zero mean and $\frac{N_0}{2}$ spectral density. The $c_l$ and $\tau_l$ parameters, $l = 1 \dots L$, characterize the channel impulse response.

The length of the ideal emitted signal is Z, the length of the received signal is M , where $Z < M$. The received signal is written as a vector:

$$r = W(\tau)c + n \tag{17}$$

Where $W(\tau) = [w^{(D_1)}, w^{(D_2)} \dots . w^{(D_l)}]^T \in R^{MxL}$ represents the matrix of the delayed versions of $w(t)$ and $w^{(D_l)} = [0_{D_l}, w, 0_{M-Z-D_l}]^T$ , with $D_l$ the discretized version of time delay $\tau_l$.

The amplitudes and delays are iteratively estimated, based on the subtraction of the first found path from the received signal, resulting in the residual signal.

The signal to noise ratio of the residual signal is iteratively maximized by a matched filter. The parameters for the strongest path are estimated from the absolute output values of the Matched Filter.

The estimated delay is determined by suppressing the matched filter delay, thus by the difference of the sample corresponding to the largest peak $k_1$ and the length Z of the ideal waveform $w(t)$ .

$$\hat{\tau}_{k_1} = k_1 - Z \tag{18}$$

The amplitude estimate $\hat{c}_{k_1}$ of the strongest path is calculated as :

$$\hat{c}_{k_1} = (w^{(k_1)^T} w^{(k_1)})^{-1} \; w^{(k_1)^T} r \tag{19}$$

Where $(w^{(k_1)^T} w^{(k_1)})^{-1} \; w^{(k_1)^T}$ is the pseudoinverse matrix of $w(\tau_{k_1})$.

The residual signal $r'$ results by subtracting the current strongest path from the received signal and the algorithm is repeated until all the paths are found.

$$r' = r - \hat{c}_{k_1} w^{(k_1)} \tag{20}$$

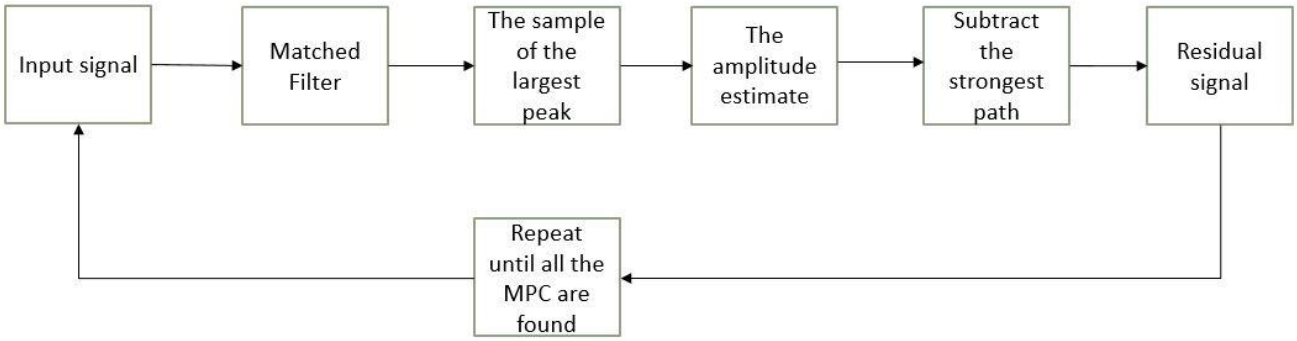


Figure 5 Steps of the algorithm

## 2.5.1 SSR Model Validation

The SSR model validation is performed on synthetic signals, the channel impulse response being given as reference. The generated waveform is the second Gaussian derivate $g(t)$, where t represents the fast time and $t_p$ represents the pulse width.

$$g(t) = \frac{1}{\sqrt{2\pi}}\left(1 - \frac{t^2}{{t_p}^2}\right) e^{\frac{-1}{2}\frac{t^2}{{t_p}^2}} \tag{21}$$

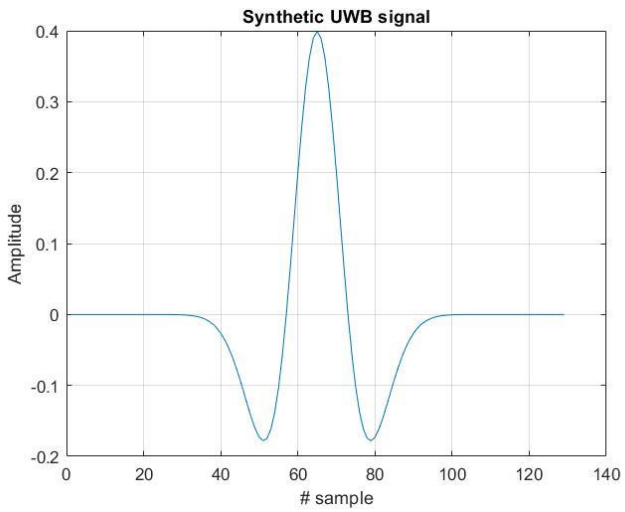


Figure 6 Second Gaussian derivate waveform

The bias of an estimator represents the difference between the average of the estimated values and the original ones, and the variance tells us how spread the data are.

$$\text{Bias}(x|\theta) = \mathrm{E}_{x|\theta}[\hat{\theta} - \theta] \tag{22}$$

$$\text{Variance}(\theta) = \mathrm{E}[(\hat{\theta} - \mathrm{E}[\hat{\theta}])^2] \tag{23}$$

Where

$\theta$ : the true values

$\hat{\theta}$ : the estimated values

E : the expected value (the mean value)

To calculate the biases and the variances for the parameters estimates, an interval of SNR values of [-10, 0], where 1000 Monte Carlo trials are considered.

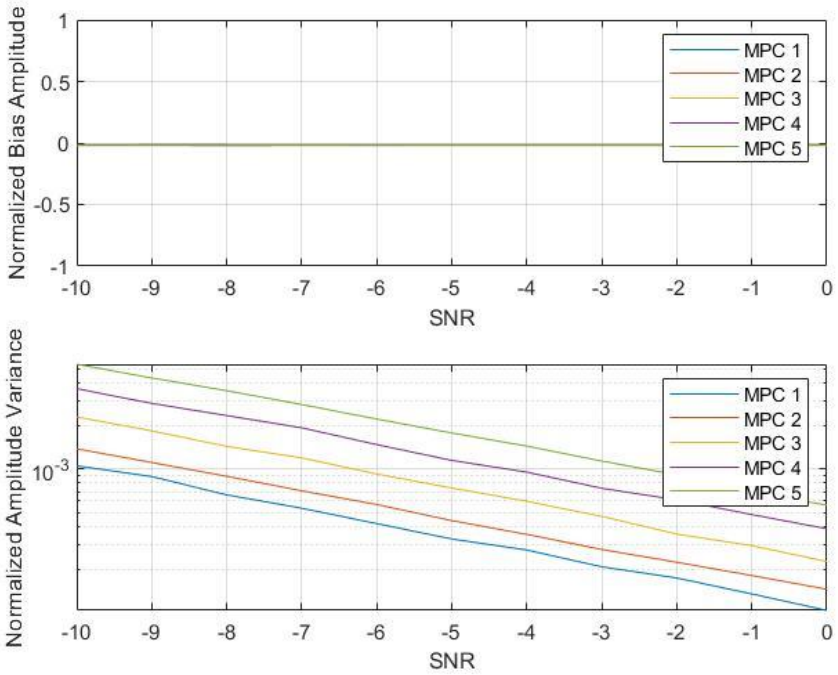


Figure 7 Biases and variances for the amplitudes

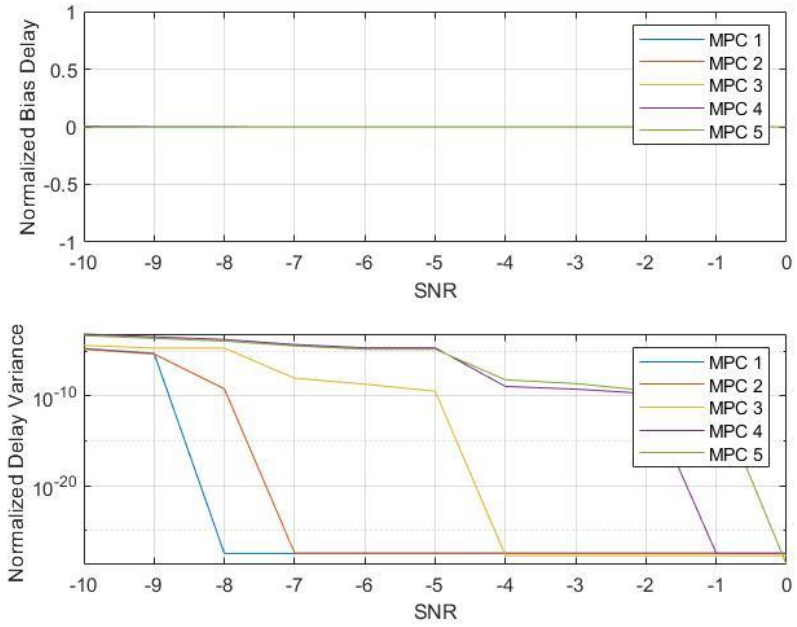


Figure 8 Biases and variances for the delay estimates

The delay estimator is unbiased and the variances decrease, SNR does not affect the delay estimation, due to the matched filter. Regarding the amplitudes, they are directly affected by the SNR. The edge of the normalized histogram is compared to a Weibull Distribution probability density function and the Normal Distribution probability density function, and it is observed that amplitude estimates follow a Normal Distribution, an observation validated by Chi-squared and Kolmogorov Smirnov statistical tests.

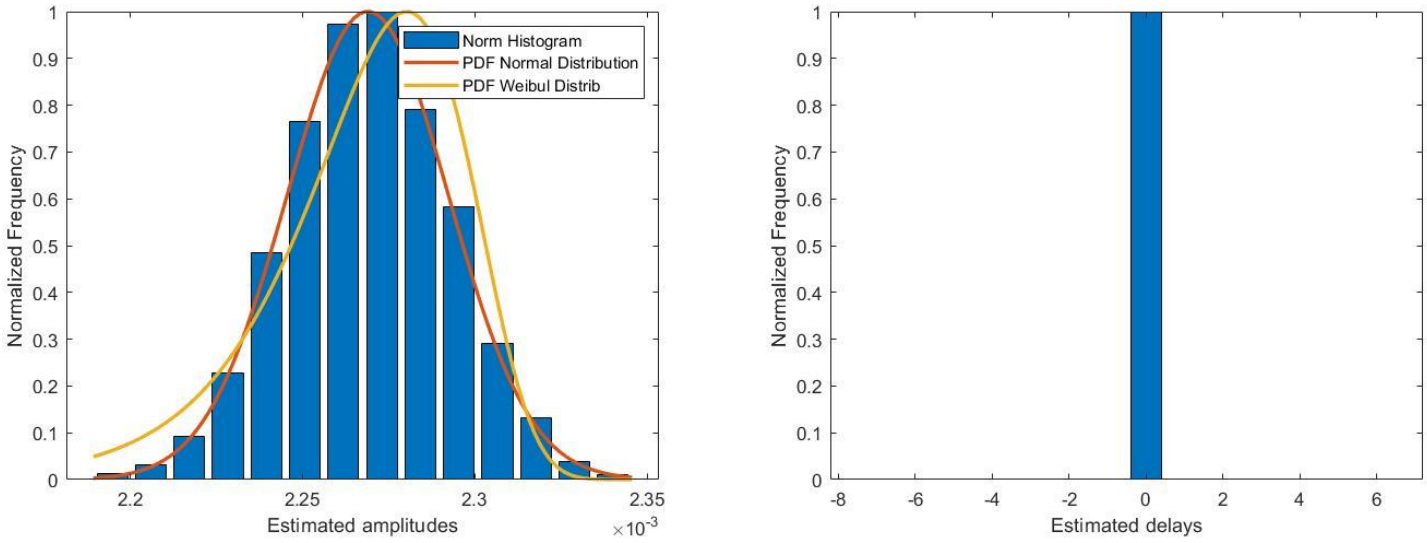


Figure 9 The normalized histograms for amplitudes and delays

The delays seem to follow a uniform distribution, thus the impact of the signal to noise ratio is less powerful than in the case of the amplitudes, due to the use of the matched filter.

Kolmogorov Smirnov test relies on the distance between the two curves in the figure above, which represents the empirical cumulative distribution function of our data and the normal distribution cumulative distribution function.

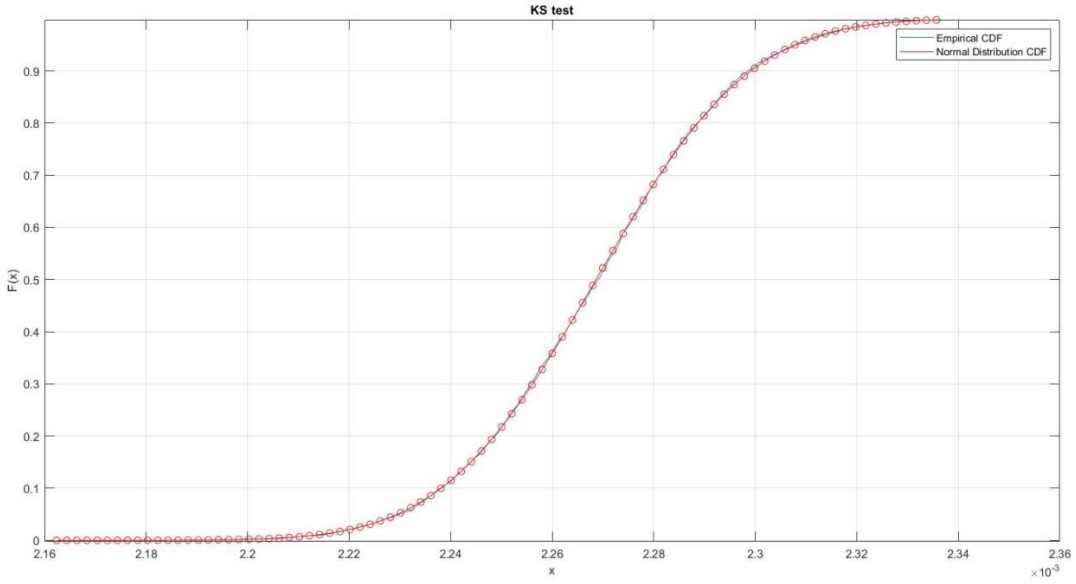


Figure 10. Kolmogorov Smirnov test

To determine the estimator's performance and efficiency, the variances are compared to the Cramer Rao Lower Bound, which is the lowest bound of the variance of an unbiased estimator.

The Normal distribution probability density function:

$$f(x) = \frac{1}{\sigma\sqrt{2\pi}} e^{-\frac{1}{2}\left(\frac{x-\mu}{\sigma}\right)^2} \tag{24}$$

where μ is the mean of data and σ is the standard deviation of the noise.

The Cramer Rao Lower Bound variance:

$$\sigma_{CR}^2 = -\left[\frac{\partial^2}{\partial^2 \mu} \ln\left(f(x,\mu)\right)\right]^{-1} =$$

$$= -\left[\frac{\partial \ln\left(f(x,\mu)\right)}{\partial \mu}\left(\ln\left(\sigma\sqrt{2\pi}\right) + \frac{(x-\mu)^2}{2\sigma^2}\right)\right]^{-1} = -\left[\frac{-1}{\sigma^2}\right]^{-1} = \sigma^2 \tag{25}$$

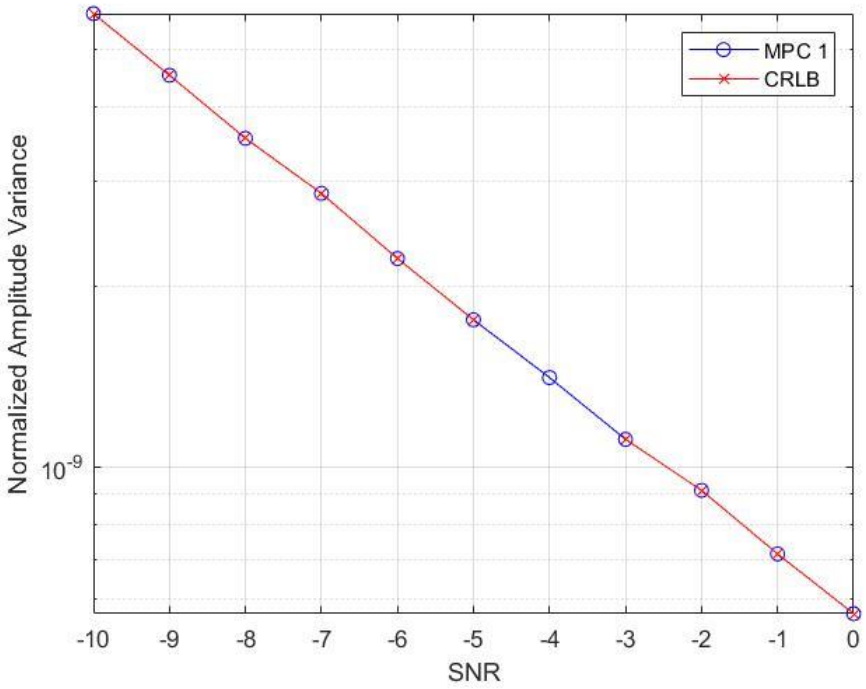


Figure 11 CRLB and Variances of the first MPC

The efficiency of the estimator is given by the ratio of the Cramer Rao Lower Bound and the variance of the estimator, which is almost equal to one.

# Chapter 3

## People detection and counting using and IR-UWB radar based on Artificial Intelligence Algorithm

This chapter presents an application of UWB signals. The application refers to people detection and counting using an IR-UWB radar based on Artificial Intelligence Algorithms such as K-nearest neighbours (KNN), Support Vector Machine (SVM), Multilayer Perceptron Neural Network (MLP) and Convolutional Neural Network (CNN).

Three methods are proposed for people classification. First approach implies the use of complex feature-extraction algorithm such as Curvelet transform for frequency-based features, the segmented-based feature extraction method for time-based features and Principal Component Analysis applied on the final set of features. For these sets of features, K-nearest neighbours, Support Vector Machine and Multilayer Perceptron Neural Network algorithms are used for classification, with the mention that both the scenario and the number of persons in the radar range are considered in the label set.

The second approach is based on a Convolutional Neural Network applied on the raw dataset of radar samples, without prior feature extraction.

The third methods proposes the use of Principal Component Analysis for data compression, both of the entire set of data and the set of extracted hybrid features, using KNN, SVM, MLP and CNN. For the two datasets, two architectures are proposed for CNN, with the mention that only the number of persons is considered in the label set.

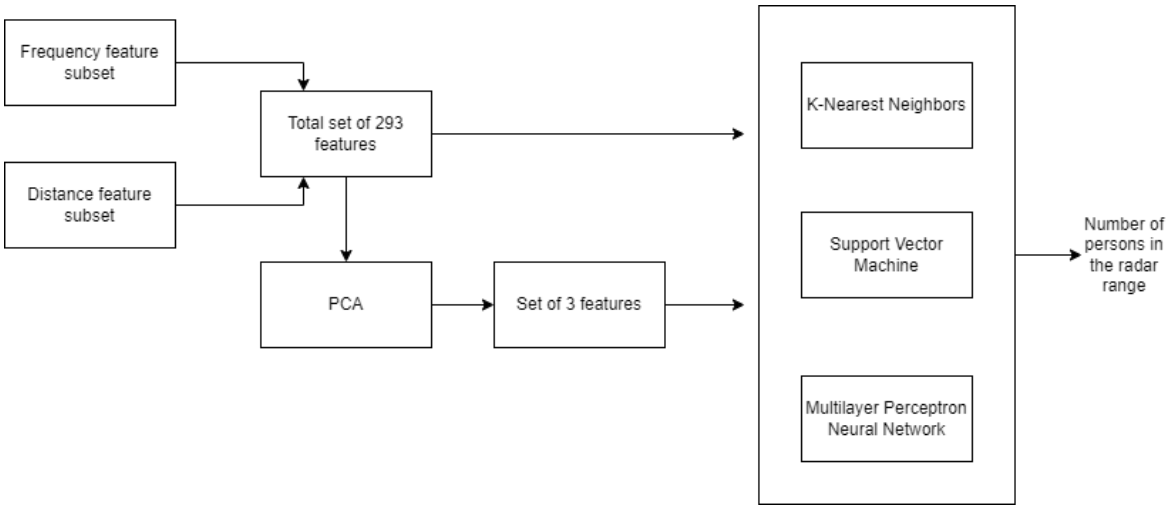


Figure 12. Block diagram of the first approach

## 3.1 State of the art of Human Detection and Classification Methods using radar technology

In literature, some methods are proposed for human detection, human activity classification, human gesture recognition, and moving target tracking. Usually, people detection and further classification is done using micro-Doppler signatures [31] [41] [14] [16] or by detecting the local maxima in the received signals [24] as extracted features.

Paper [31] uses micro-Doppler signatures of human walking gait, where a roof-top X-band radar is used for measurements. The body Doppler shift and micro-Doppler modulation of the arms` movement is detected by applying STFT to the input signals [31]. The human gait is highlighted using the superposition of the time-frequency signatures over all range cells, which gives a full time-frequency signature of a walking person.

In paper [24], a 2D IR-UWB Radar System is used for the detection, localization and tracking of a moving target. As discussed in this paper, some methods suggested for clutter and noise filtering are: Exponential Averaging (EA)

which uses the previously estimated signals for clutter estimation, and Singular Value Decomposition (SVD) which is an efficient method for through-wall applications and tracking systems, its disadvantage being an expensive computational cost, and the Kalman Filter (KF) which is finally implemented.

The targets are detected due to the comparison of signal strength with a threshold. Two decisions are made regarding the presence of the target, depending on the signal strength. The presence of the target is given by a greater signal strength, the absence being given by a weak signal strength, relative to a threshold [24].

The target distance, material and shape negatively influence the pulse waveform, which affects the matching ratio of the echo signal and a template pulse [24]. To overcome this problem, Constant False Alarm Rate (CFAR) is proposed in [42], its disadvantage being the difficulty of choosing the threshold, depending on the clutter distribution [24]; and the CLEAN algorithm which provided the optimum results, presuming the comparison of the cross-correlation between the echo and the template signal with a given threshold.

A Specular Multi-Path Model (SMPM) together with Multi-target Tracking Technique (MTT) for human body scattered UWB waveforms characterization, and human presence detection, respectively, is proposed in the paper [21]. The authors concluded that UWB radar-based human detector provides accurate results, with more than 80% detection probability and with 1.58% false alarm rate in a realistic outdoor environment. A way to improve the proposed method is the use of a hidden Markov model [21].

Paper [41] shows the effectiveness of using deep neural networks (DNN) for recognizing the micro-Doppler radar signals generated by human walking and background noises, proposing two types of DNN classifier: a binary classifier, with 97.5% classification accuracy and a DNN (Deep Neural Network) multiclass classifier, showing 95.6% accuracy.

A new approach is made in paper [14], where deep convolutional neural networks (DCNNs) are applied to raw micro-Doppler spectrograms for human

detection and activity classification. The measurements are done by a Doppler radar, in an outdoor environment and under line-of-sight conditions. It was concluded that, without any knowledge of the input data features, DCNNs provide high accuracy, with results of 97.6 % for human detection and 90.9% for human activity classification [14]. The vulnerabilities of this method could be a degrading performance due to irregularity in motions and the computational complexity in real-time applications [14].

An automotive radar of 79 GHz is used in paper [16] for pedestrian detection using the micro-Doppler signatures of the human body in the near field (0-15 m). A multi-objective optimization based on Genetic Algorithm (GA) and Random Search (RS) methods is considered for the radar parameters, improving the quality of the radar signal, by improving the velocity resolution of 0.12m/s. The Support Vector Machine (SVM) method is used for object classification: pedestrian or non-pedestrian, providing an accuracy of 99.5%

Conventional detection methods propose the comparison of the received signal power with a fixed or adaptive threshold [41]. The disadvantages of these methods are a high false alarm rate due to noise sources and a radar cross-section fluctuation of targets which degrade the detection performance [41]. New methods of human detection based on machine learning are recently developed, showing high detection accuracy.

## 3.2. People detection and counting based on Artificial Intelligence Algorithms

This subchapter presents the original dataset of radar samples, the data preprocessing, the feature extraction methods and the classification methods mentioned in the beginning of the chapter.

### 3.2.1 Dataset

The paper [18] is used as a reference, where dense human counting is performed using an NVA-R661 IR-UWB radar, with an emission pulse having a central frequency of 6.8 GHz and a bandwidth of 2.3GHz. The echo signals are received at a sampling frequency of 39GHz. Curvelet transform and Distance bin method are used as feature extractors, resulting a set of 300 features. The machine learning algorithms used for people counting are Decision Tree, AdaBoost, Random Forest and a Neural Network. The highest performance is given by the RandomForest algorithm, in the case of the second scenario, detailed below, where the accuracy is 98.7%.

A database of radar signals is constructed in [18], corresponding to four scenarios: first scenario when there are 0 to 10 people randomly walking in a radar range of 5 meters, the second scenario where there are 11 to 20 persons with a density of 3 persons per squared meter, the third scenario where there are 11 to 20 persons with a density of 4 persons per squared meter and the last scenario where 0-15 persons are standing in a queue, at a distance of 10 cm one to another.

Table 2 Dense people counting scenarios

| Scenario | Number of persons | Action |
|---|---|---|
| 1 | 0 to 10 | Randomly walking in the radar range |
| 2 | 0 to 15 | Standing in a queue with an average of 10 cm between persons |
| 3 | 11 to 20 | Randomly walking in the radar range, with a density of people of 3 persons per squared meter |
| 4 | 11 to 20 | Randomly walking in the radar range, with a density of people of 4 persons per squared meter |

The entire dataset is composed of 319000x1280 samples, meaning 6380 radar samples. A radar sample consists of 50 received signals, where a single received signal is a vector of 1x1280 samples. One radar sample of 50 received signals corresponds to a range of 5 meters on the x-axis and 1.25 seconds on the y-axis.

### 3.2.2 Data preprocessing

The data are preprocessed to remove the noise. First, the direct current component is removed from all the signals, by extracting the mean of the signal's values, and then a digital bandpass filter is applied, with the cutoff frequencies of 5.65GHz and 7.95GHz. On the resulted filtered signals, the Running Average method is applied to remove the clutter in the radar sample.

The Running Average method implies a series of averages of subsets of data with a fixed length from the total dataset. The subsets are shifted forward, excluding the first values of the series and including the next ones. Running average method acts as a low-pass filter for the data, where data become smoother.

Suppose $p_j$ data points from a dataset, where $j = \overline{1,n}$. The mean of the last $k$ data points $SMA_k$ is computed as:

$$SMA_k = \frac{1}{k}\sum_{i=n-k+1}^{n} p_i \tag{26}$$

The next mean $SMA_{k,next}$ has the same number of data points in the mean calculation and its based on the previous computed mean:

$$SMA_{k,next} = \frac{1}{k}\sum_{i=n-k+2}^{n+1} p_i = SMA_{k,prev} + \frac{1}{k}\left(p_{n+1} - p_{n-k+1}\right) \tag{27}$$

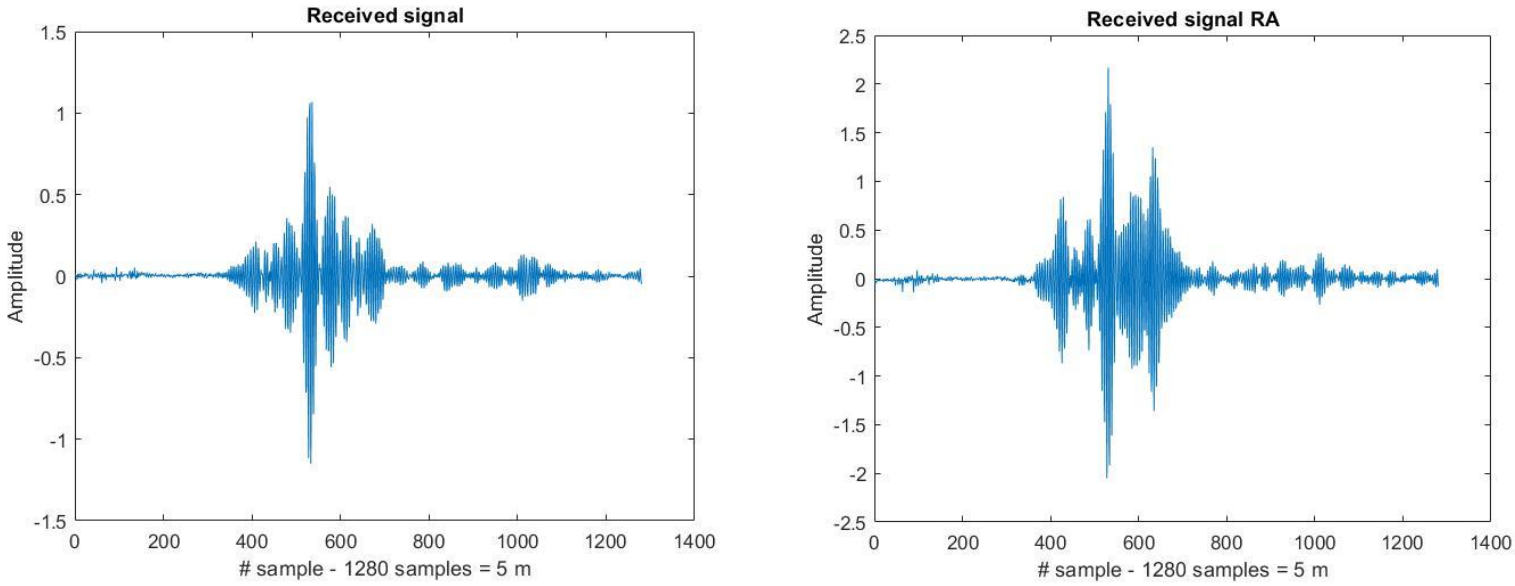


Figure 13 Received signal and clutter removed received signal

Taking as an example one signal, there can be seen that the data become smoother, the clutter is removed and the signal to noise ratio increases.

The figure below represents two cases for the first scenario: the image on the left represents a radar sample of 0 persons moving in the radar range, and the radar sample on the right represents the echo signal for 10 persons randomly walking in the radar range.

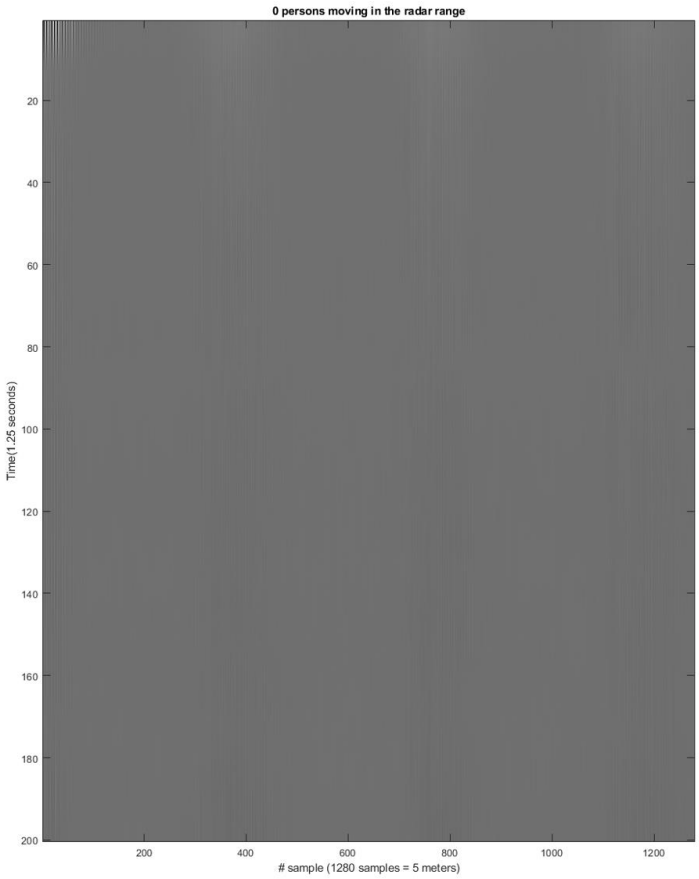


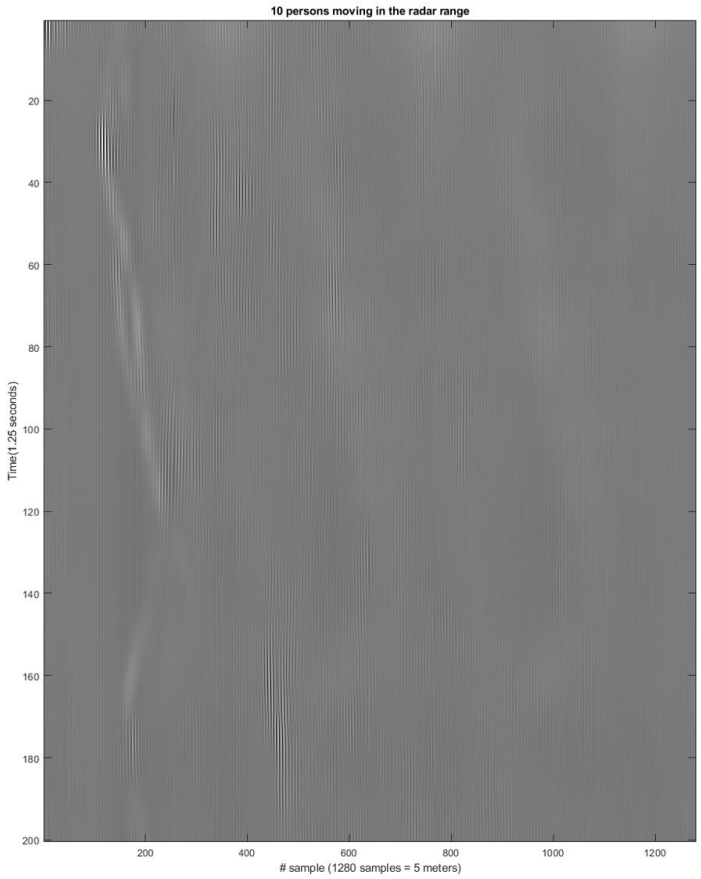


Figure 14 a) 0 persons moving in the radar range b) 10 persons moving in the radar range

The next figure represents two radar samples from the second scenario. The image on the left represents the echo signal for 5 persons standing in the queue, with 10 cm distance between them, and the right image represents the echo signal for 15 persons standing in the queue, with 10 cm distance between them.

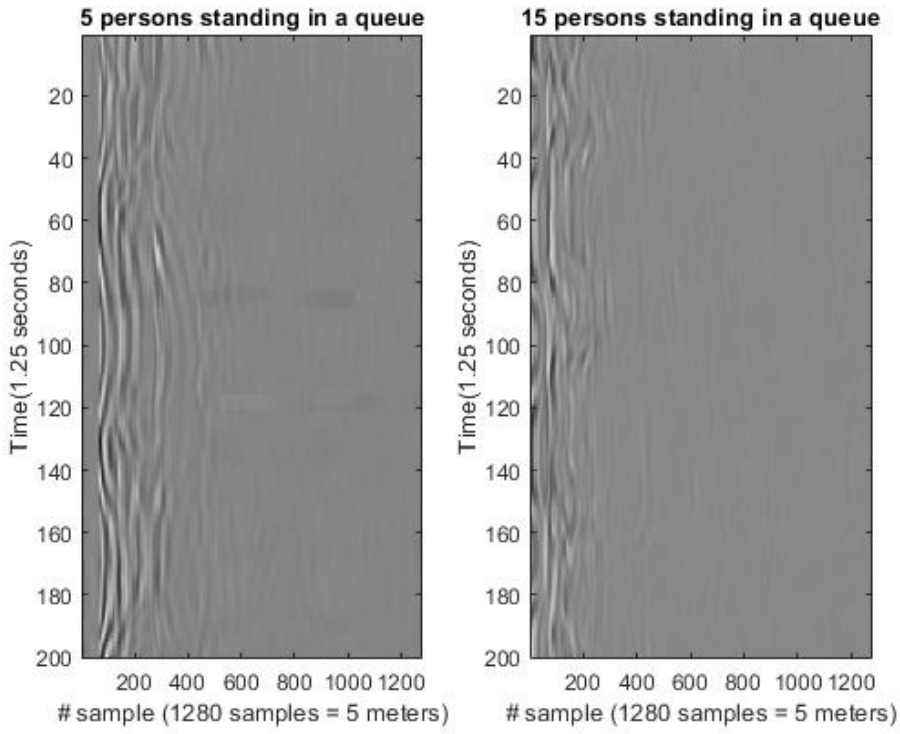


Figure 15 a) 5 persons standing in a queue b) 15 persons standing in a queue

The next figure represents two radar samples from the third scenario. The image on the left represents the echo signal for 11 persons walking in the radar range, with a density of three persons per square meter, the right image represents the echo signal for 20 persons walking in the radar range, with a density of three persons per squared meter.

The figures below represent two radar samples from the last scenario. The image in the left represents the echo signal for 11 persons walking in the radar range, with a density of four persons per square meter, the right image represents the echo signal for 20 persons walking in the radar range, with a density of four persons per squared meter.

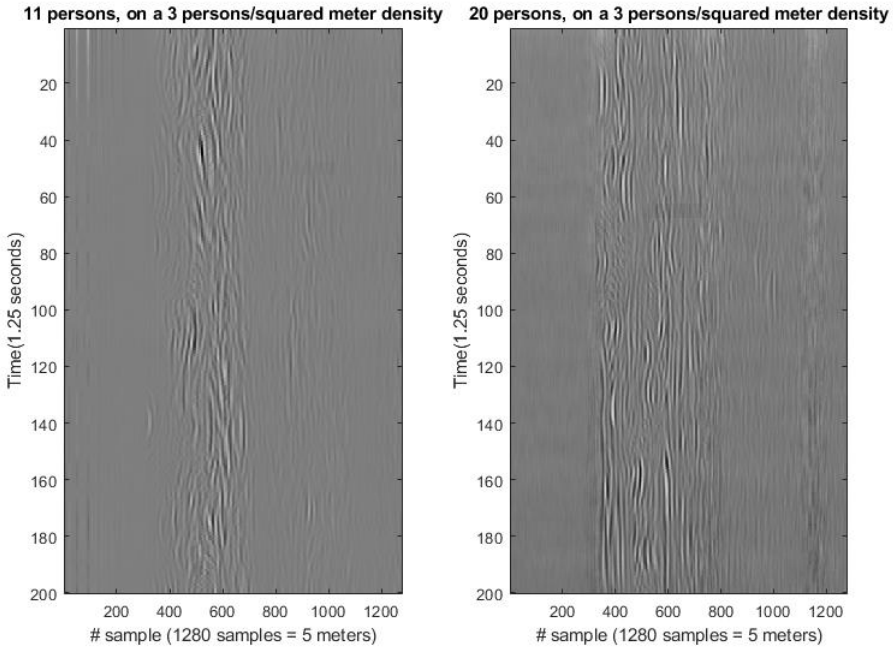


Figure 16 11 and 20 persons walking in the radar range, with a density of three persons per squared meter

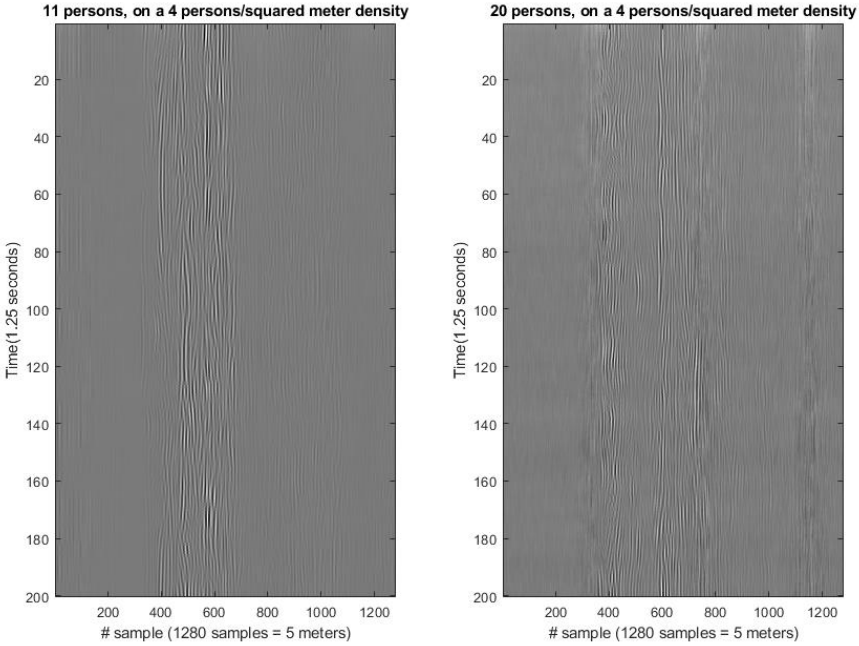


Figure 17 11 and 20 persons walking in the radar range, with a density of four persons per squared meter

### 3.2.3 Feature extraction

The Curvelet transform feature extraction implies Fast Discrete Curvelet Transforms computation, using the wrapping method [19], on the preprocessed radar samples. Energy and amplitude features are extracted from the coarse, detail and fine layers.

The segmented-based feature extraction method feature extraction method implies the segmentation of each received signal in fixed-length segments of 32, 64, 128 samples (corresponding to a 125, 250 and 500 mm distance). Energy and amplitude features are extracted from every segment, both from the preprocessed signals and the clutter removed signals.

#### 3.2.3.1 The Curvelet transform

Curvelet transform represents a multi-scale orientation-selective analysis algorithm, first proposed by Candes and Donoho, and it is mostly used for image processing due to its capability of anisotropy, strong direction and efficiency of image edge representation [43].

The curvelet transform equation involves three parameters: the scale $j$, the direction $l$ and the position $k$:

$$C(j,l,k) = \int \hat{f}(\omega)\widehat{U}_j(S_{\theta_l}^{-1}\omega)e^{i<S_{\theta_l}^{-T}b,\omega>}d\omega \quad (28)$$

Where the terms represent the following:

$f$ the input Fourier samples of the data in the Cartesian coordinate system

$\widehat{U}_j$ the frequency rectangle window for each scale

$S_{\theta_l}$ the shear matrix with orientation $\theta_l$, where $S_{\theta_l} = \begin{bmatrix} 1 & 0 \\ -tan\theta_l & 1 \end{bmatrix}$

$b \coloneqq (k_1 2^{-j}, k_2 2^{-j/2})$ where $k_1, k_2$ are the translation parameters taking values on a rectangular grid.

The curvelet coefficients are computed using the Inverse Fourier Transform of the multiplication of the Fast Fourier Transform of the curvelet function and the FFT of the original image. The convolution operation in the spatial domain corresponds to multiplication in the frequency domain.

$$C = IFFT\{FFT(Curvelet)\ FFT(Image)\} \tag{29}$$

Hard thresholding on energy is used in this case, and it implies energy thresholding, where the cumulative sum of the energy is computed to apply the established threshold at which the values below it would be dropped out. In our case, the curvelet coefficients whose energy is below 90% of the energy of the total coefficients, are dropped.

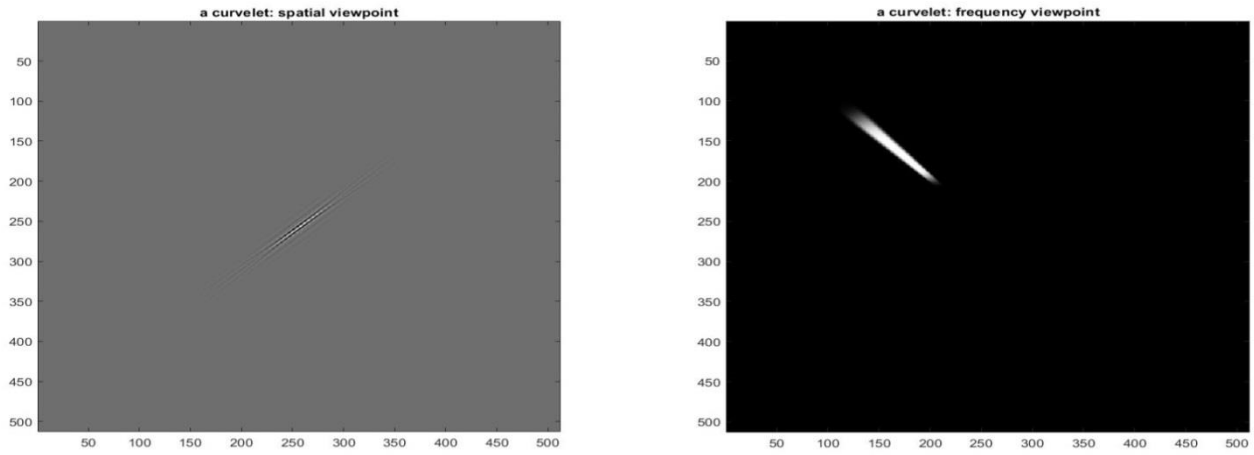


Figure 18 A curvelet in the spatial and frequency domain

The coefficients are divided into the finest layer, corresponding to the high frequencies, the detail layer and the coarse layer corresponding to low frequencies. The coarse layer provides general information about the input signal and the detail layer contains high-frequency information which provides the details [43].


Figure 19 Original image and Curvelet coefficients of the original image

The right image in Figure 27 shows the graphical representation of all the curvelet coefficients of the original image, at all scales, orientations and directions. The approximation coefficients are represented in the center of the image.

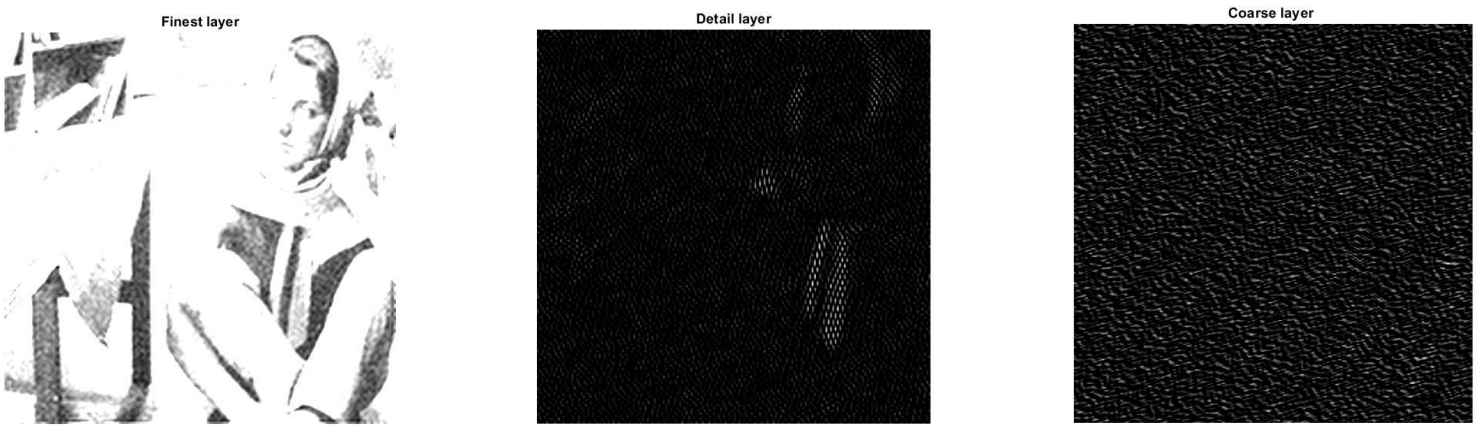


Figure 20. Coefficients on the finest, detail and coarse layer

Traditional wavelets have strong limitations concerning their effectiveness in a higher dimension than 1, because they rely on isotropic elements occurring at all scales and locations and do not describe the anisotropic elements [44]. The advantage of curvelet transform in front of wavelet transform is that it is more efficient when it comes to compression, de-noising, structure and edge extraction for features with line and surface singularities [45].

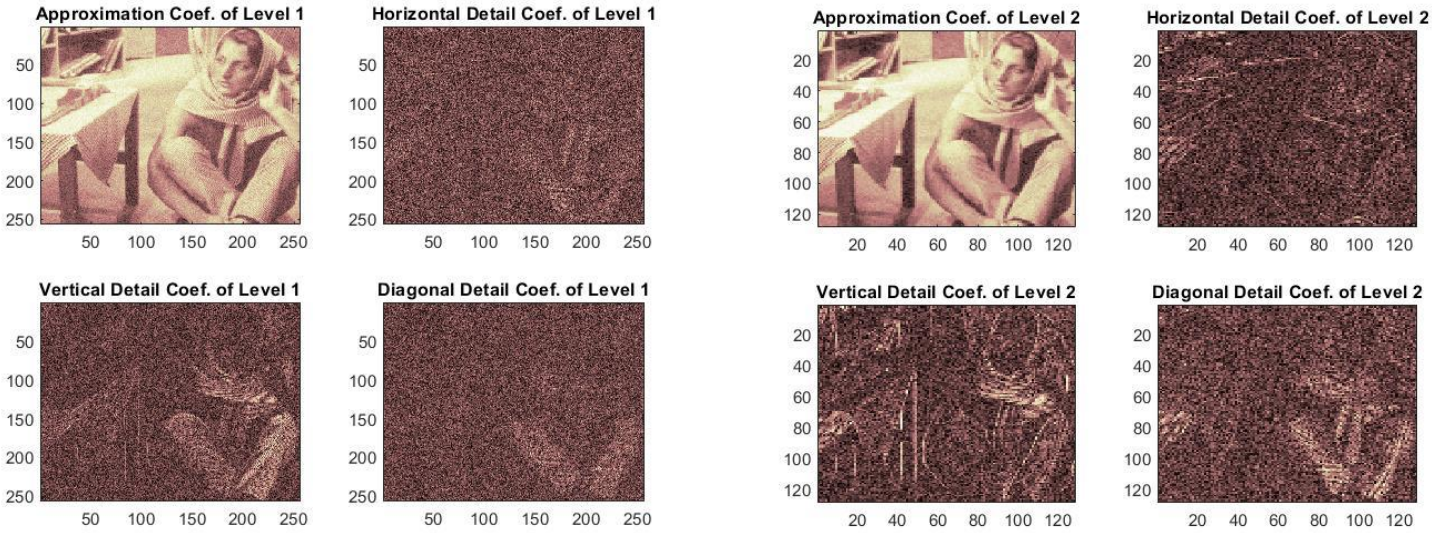


Figure 21 Coefficients of Level 1 and Level 2 using wavelet transform


Figure 22. Image reconstruction and the correspondent SNR

The original image is reconstructed and de-noised both using curvelet transform and wavelet decomposition. The signal to noise ratios in the reconstructed and de-noised images, 25.1316 for curvelet transform and 13.591 dB for wavelet transform show the effectiveness of the curvelet transform.

The FDCT via wrapping method implies the wrapping of the data, in the frequency domain, into a rectangle, initially inside a parallelogram $P_{j,l}$, which will be then centered at the origin [19].

First step is the 2D FFT computation of the data, obtaining the Fourier samples $\hat{f}[n_1, n_2]$, and for each scale j and angle l a parallelogram $P_j$ is constructed, inside where the rectangle window $\overline{U_{j,l}}[n_1, n_2]$ with dimensions $L_{1,j} = 2^j, L_{2,j} = 2^{j/2}$ is supported [19].

$$P_j = \{(n_1, n_2): n_{1,0} \leq n_1 < n_{1,0} + L_{1,j}, n_{2,0} \leq n_2 < n_{2,0} + L_{2,j}\} \quad (30)$$

Where $(n_{1,0}, n_{2,0})$ is the index of the bottom-left pixel of the rectangle. The data $d[n_1, n_2]$ are windowed by the discrete localizing window $\overline{U_{j,l}}[n_1, n_2]$, where:

$$d[n_1, n_2] = \overline{U_{j,l}}[n_1, n_2]\, \hat{f}[n_1, n_2] \quad (31)$$

The product is then wrapped around the origin, where $0 \leq n_1 < L_{1,j}$ and $0 \leq n_2 < L_{2,j}$:

$$\bar{f}_{j,l}[n_1, n_2] = W\left(\bar{U}_{j,l}\hat{f}\right)[n_1, n_2] \quad (32)$$

The discrete coefficients will be collected by applying the inverse 2D Fourier transform, 2D IFFT, for each $\bar{f}_{j,l}$.

### 3.2.3.2 The segmented-based feature extraction method

The segmented-based feature extraction method implies the segmentation of each received signal into segments of length 32, 64 and 128 samples corresponding to a 125, 250 and 500 mm distance.

The segmented-based feature extraction method is applied both on the band passed input signals and on the reconstructed signal. The energy and the maximum amplitude are extracted as features from every segment.

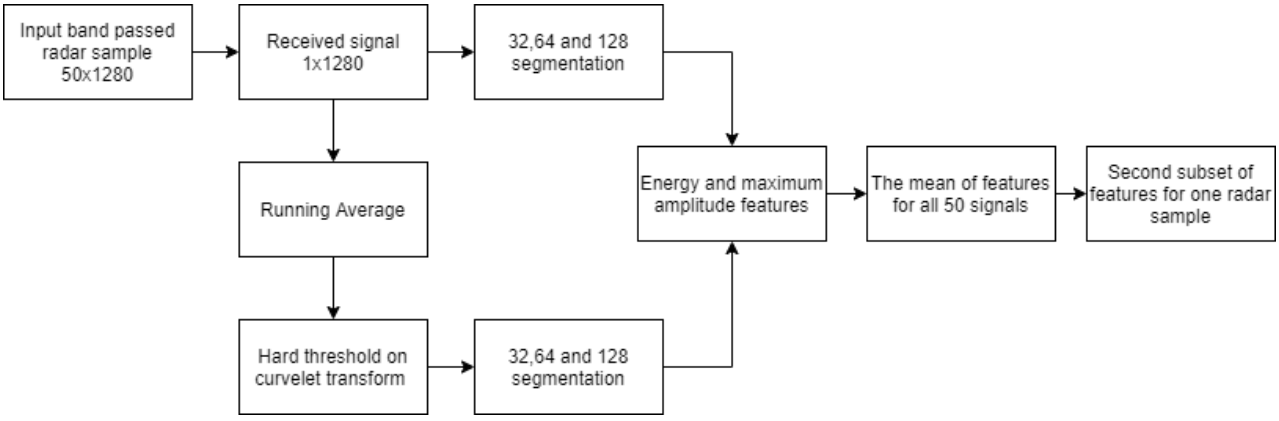


Figure 23 Block diagram the segmented-based feature extraction method

#### 3.2.3.3 Principal Component Analysis (PCA)

The principal component analysis is a method used for dimension reduction of a high dimensional dataset by keeping the most important information from the data as a set of components called principal components, which are a linear combination of the original data [46]. PCA method aims to find directions along which the variation in the data is maximal and along which the data can be projected, with minimal loss of information [46].

PCA method could be used in data which are correlated (meaning high redundancy), thus the data can be reduced to new uncorrelated variables, named principal components. The purpose of this method is to reduce the data dimensionality by removing the noise and redundancy, finding hidden patterns and identifying correlations in the dataset [46].

The main advantages of this method are that it provides uncorrelated vectors as outputs (principal components) and that it reduces the dimensionality of the data, by keeping most of the energy, mainly compressed in the first principal component.

The Principal Component Analysis relies on the computation of the eigenvector and eigenvalues of the covariance matrix of the original data. The covariance matrix is a symmetric matrix that shows correlations in the data. The main diagonal of this matrix represents the variances of the variables in the data.

The first principal component is the line that maximizes the variance of the data (the mean of the squared distances from the projected points to the origin [47] ). The second principal component will be orthogonal to the first one, and it has the next higher variance.

The eigenvectors of the covariance matrix give the direction of the axes which has the most variance and the eigenvalues give the amount of the information in each principal component [47]. Each eigenvector has an eigenvalue and the highest eigenvalue corresponds to the first principal component, and so on,

in descending order. The amount of information in each principal component is given by the division of the eigenvalue of the principal component and the sum of all eigenvalues.

Suppose the original data matrix X, the covariance matrix $C_X$ is given by:

$$C_X = E[(X - E[X])(X - E[X])^T] \quad (33)$$

Where $E[\,]$ represents the expected value, or the mean value and T is the transpose operation of a matrix.

"If T is a linear transformation from a vector space V over a field F into itself and v is a nonzero vector in V, then v is an eigenvector of T if T(v) is a scalar multiple of v. This can be written as: $T(v) = \lambda v$, where $\lambda$ is a scalar in $F$, known as the eigenvalue, characteristic value, or characteristic root associated with v." [48]

To construct the feature vector $E$ (given by the highest eigenvalues of the covariance matrix) and to reduce the dimensionality of the data, a threshold is used for discarding the principal components that have the lowest amount of information (given by the corresponding lowest eigenvalues).

The final dataset $Y$ is constructed based on the multiplication of the transpose of the original dataset $X$ and the transpose of the feature vector.

$$Y = X^T E^T \quad (34)$$

In our case, Principal Component Analysis is applied to the feature matrix extracted from the original dataset of the radar data to reduce the dimensionality of the data, avoid over-fitting and improve the computational cost and speed of the training process of the classifiers.

Suppose $X$ – the original matrix of the non-normalized features of size $(M\ x\ N)$. The extracted features are normalized using the amount of energy within it. For each subset of features $X_i$, $i = \overline{1,n}$, $n$ the number of subsets of features, the autocorrelation matrix is computed:

$$R_{xx} = \frac{1}{N}(X_i{}^T X_i) \quad (35)$$

Then a diagonal matrix $K_n$ is constructed, having as elements the squared root of the inverse of the sum of the main diagonal elements of the autocorrelation matrix (representing the energy in the signal). The final normalized dataset will be $Y_i = X_i K_i$.

The $K_i$ matrixes are saved for future normalization of the new data's subsets of features. The final normalized dataset is constructed by putting together all the $Y_i$ matrixes.

### 3.2.4 People counting based on Artificial Intelligence Algorithms

Machine Learning is a branch of Artificial Intelligence (AI). Machine Learning algorithms learn from the data and provide accurate outputs when it comes to new data, based on what it has learned from the training data. The data are split into training data, from which the algorithm learns, data and test data, which are used to test the algorithm performance and evaluation.

In AI, there could be supervised and unsupervised learning algorithms, which consist of models trained to find patterns and correlations in the data. Briefly, supervised learning algorithms learn from the training data having the given targets or labels, while unsupervised learning algorithms find patterns in the training data and provide output classes on their own.

In our case, we use supervised learning for people counting. The final features dataset and its corresponding matrix of labels from 0 to 20 (corresponding to the scenario and number of persons) are used as input for the classifiers, to provide the number of persons in the radar range. The dimension reduction for the initial dataset improves the computational cost and speed of the training process and avoids over-fitting.

In this chapter, four Artificial Intelligence algorithms (K-nearest neighbours, Support Vector Machine, Multilayer Perceptron Layer and Convolutional Neural Network) used for people counting are briefly presented.

### 3.2.4.1 K-nearest neighbours

K-nearest neighbours is a supervised machine learning algorithm used both for regression and classification. This algorithm is based on similarity (or distance) between surrounding points, where Euclidean distance is mostly used. The K number of "neighbours" is given by the user, the bigger the K, the smaller the effect of the noise, but the lesser distinctions between classes. The algorithm's output for new input data relies on the dominant class among its neighbours (samples in the training set).

Suppose two points $A(a,b), B(c,d)$, the Euclidean distance $d(A,B)$ from A to B is the following:

$$d(A,B) = \sqrt{(a-c)^2 - (b-d)^2} \tag{36}$$

### 3.2.4.2 Support vector machine (SVM)

Support Vector Machine is a supervised machine learning algorithm used for classification and regression, widely used in industry and science. The algorithm relies on splitting the data with hyperplanes and projects them into higher dimensions.

There are several approaches for SVM: Linear SVM, Nonlinear SVM and Kernel Methods. SVM aims to optimize the largest margin between the data [49].

The Linear SVM constructs a hyperplane: $w * x + b = 0$, where each hyperplane has a different value of w and the constant b, which optimally separates the labelled data [49]. Given a new data point $x_j$, it can be classified by computing the sign of $w * x_j + b$.

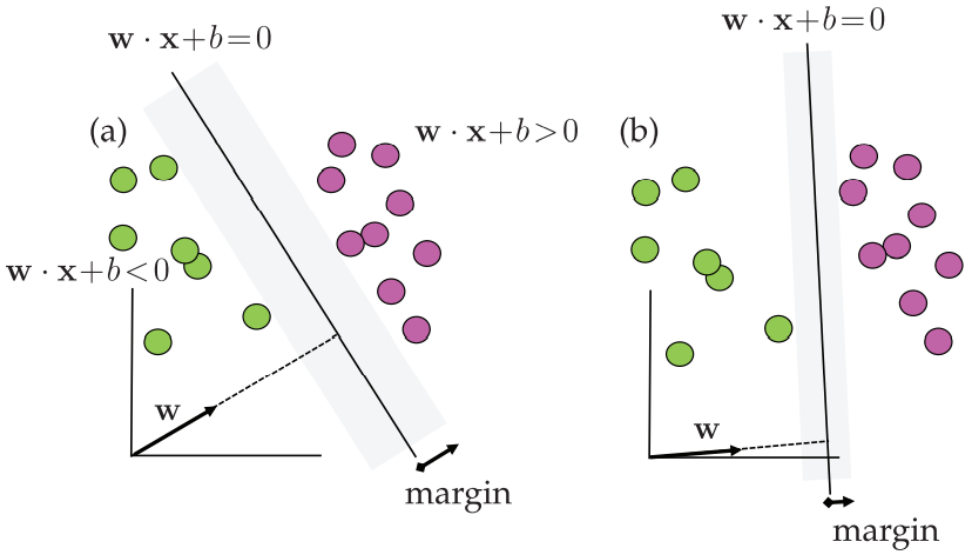


Figure 24 SVM Classification scheme [37]

The support vectors are given by the vectors which touch the edge of the grey regions.

The Nonlinear SVM is one of the most successful machine learning algorithms and it maps the data into a new, nonlinear, higher-dimensional space by including new enriched nonlinear features to build more sophisticated classification curves. The hyperplane function is given by :

$$f(x) = w\,\varphi(x) + b \tag{37}$$

Considering two data points $x = (x_1, x_2)$. The new space of data will be:

$$(x_1, x_2) = \ (z_1, z_2, z_3) \coloneqq (x_1, x_2, x_1^2 + x_2^2) \tag{38}$$

The new labelling function is given by $\overline{y_j} = sign(w\ \varphi(x) + b\ )$, where $\varphi(x)$ is the enriched space of the observed data [49].

To reduce the computation cost, kernel SVM methods are developed. The w vector is represented as $w = \sum_{j=1}^{m} \alpha_j \varphi(x_j)$, where $\alpha_j$ are the weights for the nonlinear observable functions $\varphi(x_j)$. The hyperplane function will be the following:

$$f(x) = \sum_{j=1}^{m} \alpha_j \varphi(x_j)\ \ \varphi(x) + b \tag{39}$$

The Kernel function is defined as:

$$K(x_j, x) = \varphi(x_j)\varphi(x) \tag{40}$$

The Kernel used in our case is the Radial basis function (RBF), defined as:

$$K(x_j, x) = \exp(-\gamma \|x_j - x\|^2) \tag{41}$$

Where $\gamma$ is the width of the Gaussian kernel measuring the distance between data points and the classification line [34].

### 3.2.5. Multilayer Perceptron Neural Network

Multilayer Perceptron Neural Network is an algorithm which maps the input layer to the output layer through a function that is learned while the training process. Between the input and output layer, there could be more hidden layers consisting of neurons (weights) which are updated based on the mean squared error between the real output and the actual output. In Neural Networks, the mean squared error between the given targets and the actual outputs is optimized by backpropagation methods (example: Gradient Descent).

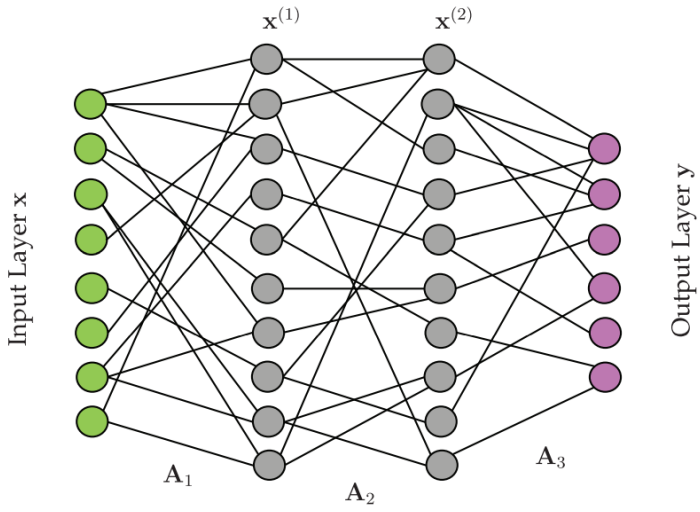


Figure 25. Two hidden layers of Neural Network Architecture [34]

In our case, the neural network has 4 layers of 50 neurons. The activation function is Rectified Linear Unit (ReLU). ReLU activation function is given as following:

$$f(x) = \max(0, x) \tag{42}$$

Where x is the neuron's input. The advantages of this activation function are that it has a sparse activation (reduces the computational cost because it makes some of the neurons inactive), better gradient propagation (for minimizing the

mean squared error between the output and the target output) and it is computationally efficient.

### 3.2.6. Convolutional Neural Network (CNN)

Convolutional Neural Networks are deep-learning algorithms that are inspired by the functioning of the human visual system and are commonly used for image classification problems. CNN architecture consists of convolutional layers, pooling layers, and fully connected layers.

The role of the convolutional layers is to extract features from the input data, which are tensors, meaning they have more than two dimensions. The results will be an activation map, or a feature map, which will be passed to the next layer. Commonly, the convolutional layers are followed by an activation function, which removes negative values from the feature map and set them to zero.

The pooling layer has the role of down-sampling the data, in order to reduce the spatial size of representation and the number of parameters. The most common pooling layer function is max pooling. The fully connected layers connect all the activations from the previous layer. The fully connected layer is usually followed by a logistic function such as SoftMax.

### 3.2.7 Metrics in model evaluation

To validate the model, some metrics are usually used in classification problems, such as accuracy, precision, recall, f1-score.

The accuracy is given by the ratio of correct predicted values and the total predicted values.

$$accuracy = \frac{nr.\ of\ correct\ predictions}{nr.\ of\ total\ predictions} \tag{43}$$

The precision is given by the ratio of true positive and the sum of true positive and false positive, where true positive refers to the case where the model correctly predicted the positive class and false positive refers to the case where the model incorrectly predicts the positive class.

$$precision = \frac{True\ positive}{True\ positive + false\ positive} \tag{44}$$

Recall function is given by the ratio of true positive and the sum of true positive and false negative, where false negative refers to the case where the model incorrectly predicts the negative class.

$$recall = \frac{True\ positive}{True\ positive + false\ negative} \tag{45}$$

F1- score function combines both the precision and recall function as follows:

$$f1score = \frac{2\ precison * recall}{precision + recall} \tag{46}$$

# Chapter 4

## Experimental work and results

This paper aimed to present some signal processing methods for ultra-wideband signals and to compare three approaches to people detection and counting using an IR-UWB radar.

The three approaches refers to the set of features extracted from the database, which first proposes a complex algorithm for frequency-based and time-based feature extraction, resulting in a set of 293 features, second proposes a Convolutional Neural Network for feature extraction and the third proposes Principal Component Analysis for data compression.

For the classification part, K-nearest neighbours, Support Vector Machine, Multilayer Perceptron Neural Network and Convolutional Neural Network are used as supervised machine learning and deep learning algorithms. The final classification consists in providing with the number of people and the radar sample. Results regarding the three methods are provided in terms of accuracy, recall, precision and f1-score functions. The simulation was done using Python programming language. K-NN and SVM were implemented using Scikit-learn Python library, MLP was implemented using Keras library and CNN was implemented using Pythorch framework.

## 4.1 Signal processing methods for UWB signals

For the analysis of the signals from UWB systems, the communication system is considered as follows:

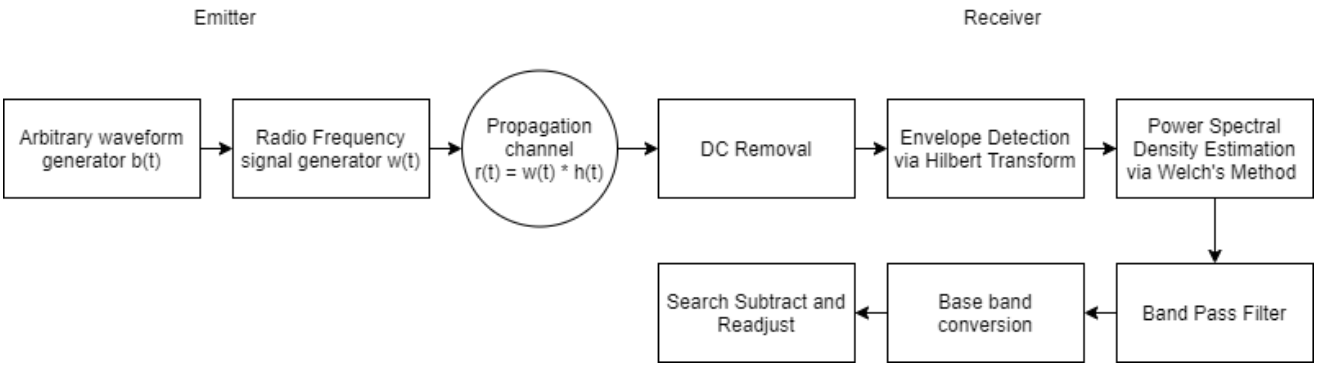


Figure 26 Communication system

The emission system proposed in our case for UWB signal generation is composed of two signal generators:

- an arbitrary waveform generator
- a radiofrequency generator.

An arbitrary waveform generator can generate any given wave shape given by the user. The arbitrary waveform generator emits the ideal UWB baseband signal with a 5 ns pulse duration and a 2 GHz bandwidth. The radiofrequency generator translates the baseband UWB signal on a central frequency of 7.25 GHz. The resulted signal is a training impulse with a 90 ns signal period, occupying a 2 GHz frequency bandwidth.

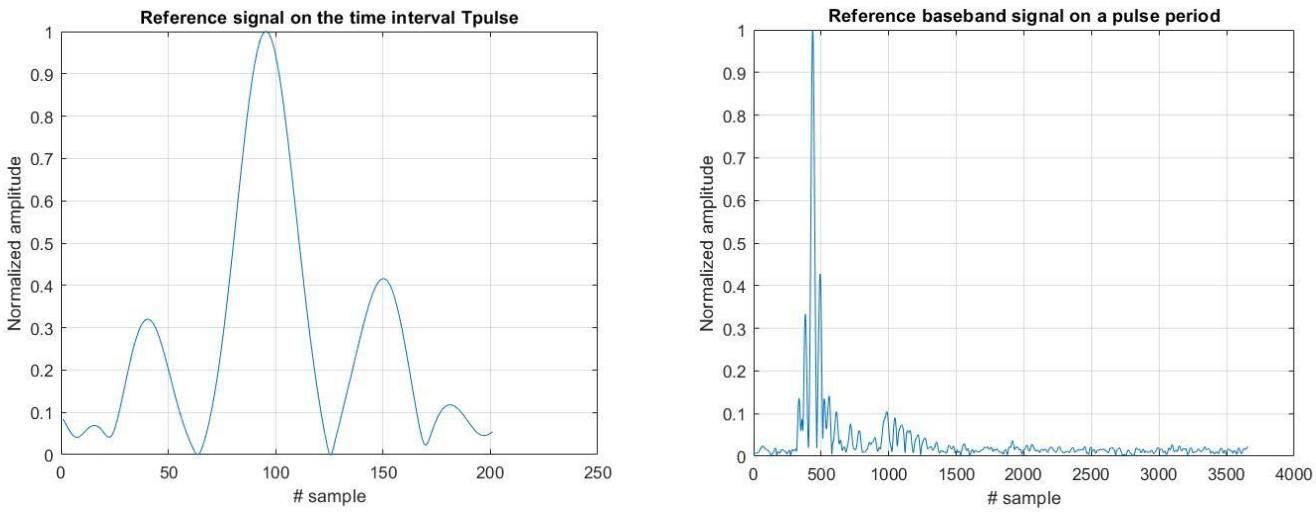


Figure 27 The reference UWB baseband signal

The signal is received using a high sampling rate oscilloscope at a sampling frequency of 40 GHz, concerning the Nyquist Rate. The effect of the propagation channel and the background noise on the wireless signal is observed in the signal to noise ratio, which is much lower in the wireless channel.

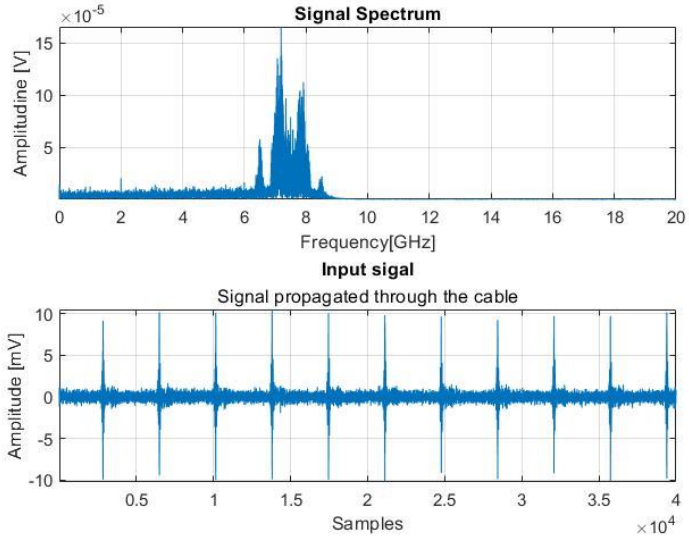


Figure 28 a. Cable signal and its spectrum

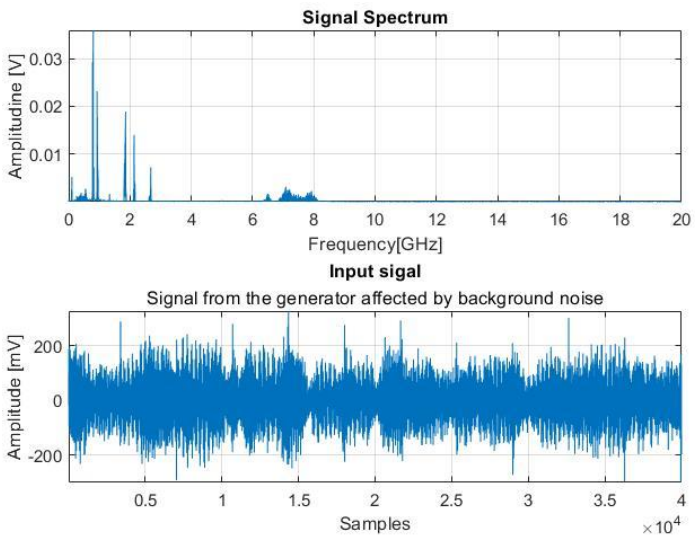


b. Wireless signal and its spectrum

The envelope detection if performed on the received signal, where the number of the signal envelope`s peaks, using a threshold of 75% of the maximum amplitude value, corresponds to the number of the signal's periods. The length of a period is the division of the total signal length and the number of periods.

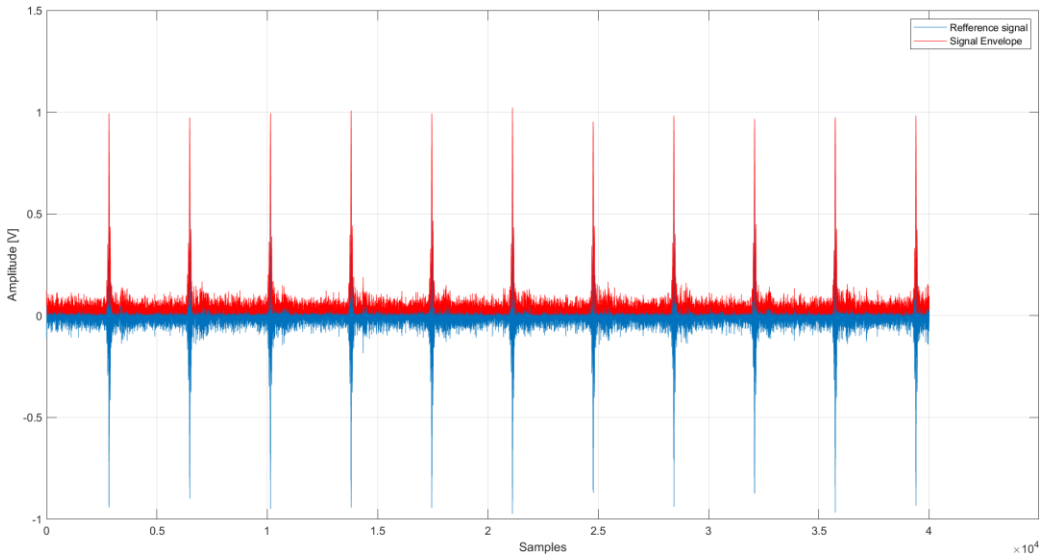


Figure 29 The original waveform and its envelope using the Hilbert transform

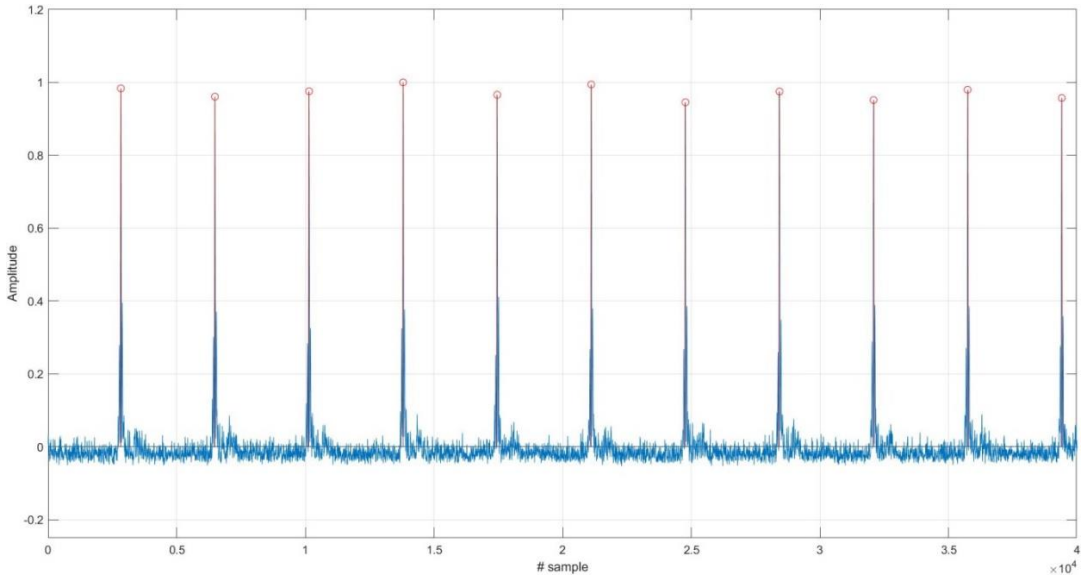


Figure 30 Finding the peaks of the signal envelope concerning a 75% threshold

To find out the signal's bandwidth, Power Spectral Density via Welch's method is performed. A bandwidth of 2 GHz is observed in the representation of the Power Spectral Density, with a central frequency of 7.25 GHz, by using a fixed threshold.

Using the 2 GHz bandwidth, a digital bandpass filter is used for filtering the input signal, having an upper frequency of 8.25 GHz and the lower frequency of 6.25GHz.

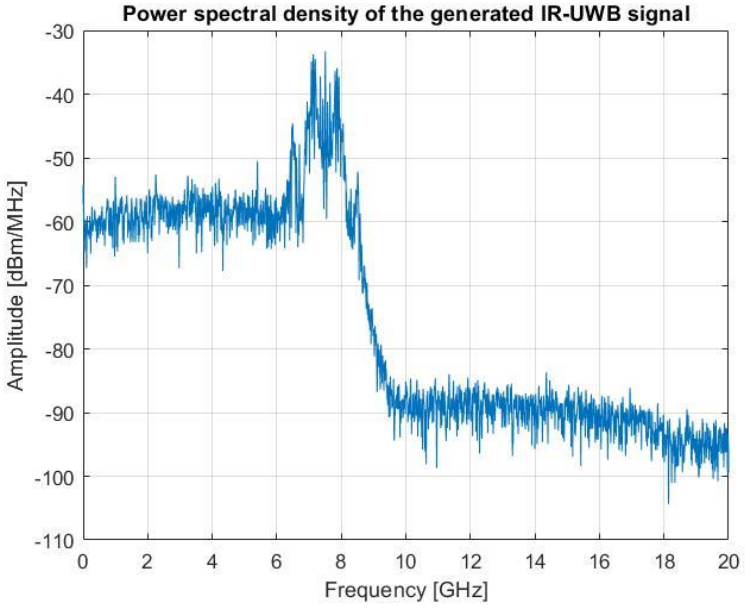


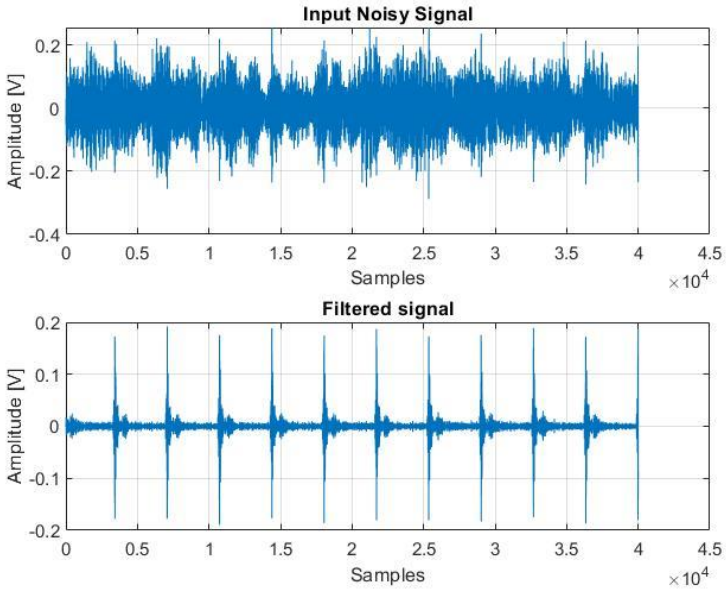


Figure 31 a. Power Spectral Density of the generated signal b. The filtered generated signal

The input signal will be converted in the baseband with the use of a frequency mixer, followed by a low pass filter, for further numerical signal processing.

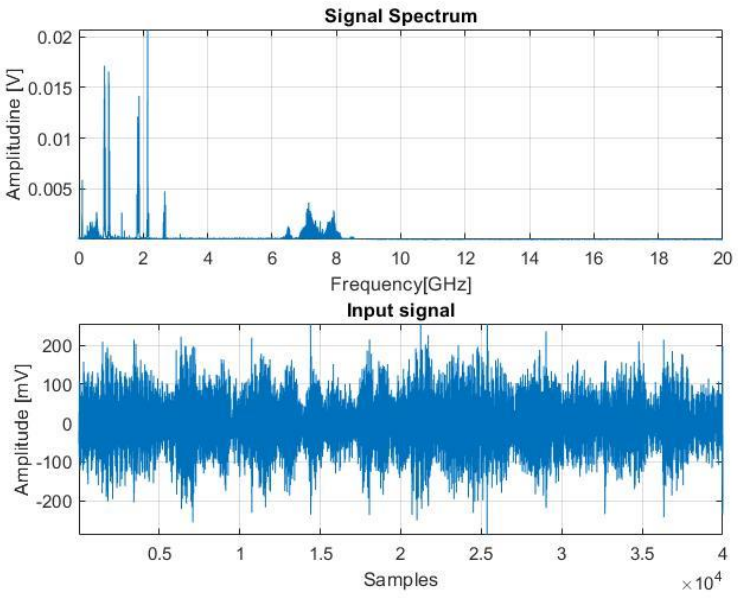


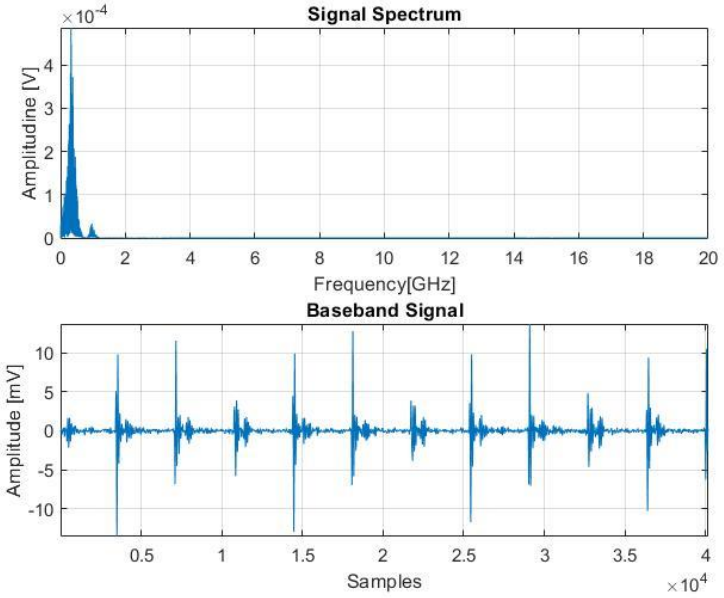


Figure 32. a. The original signal and its frequency spectrum b.The baseband signal and its frequency spectrum

To maximize the SNR and filter the UWB signal, a matched filter based on the time-reversed ideal baseband emitted signal is designed, and then the convolution between the input signal and the filter's impulse response is computed, SNR being maximum at the signal's period. The Matched Filter introduces a delay equal to the length of the reference signal, which must be suppressed for further time delay estimation of the multipath components.

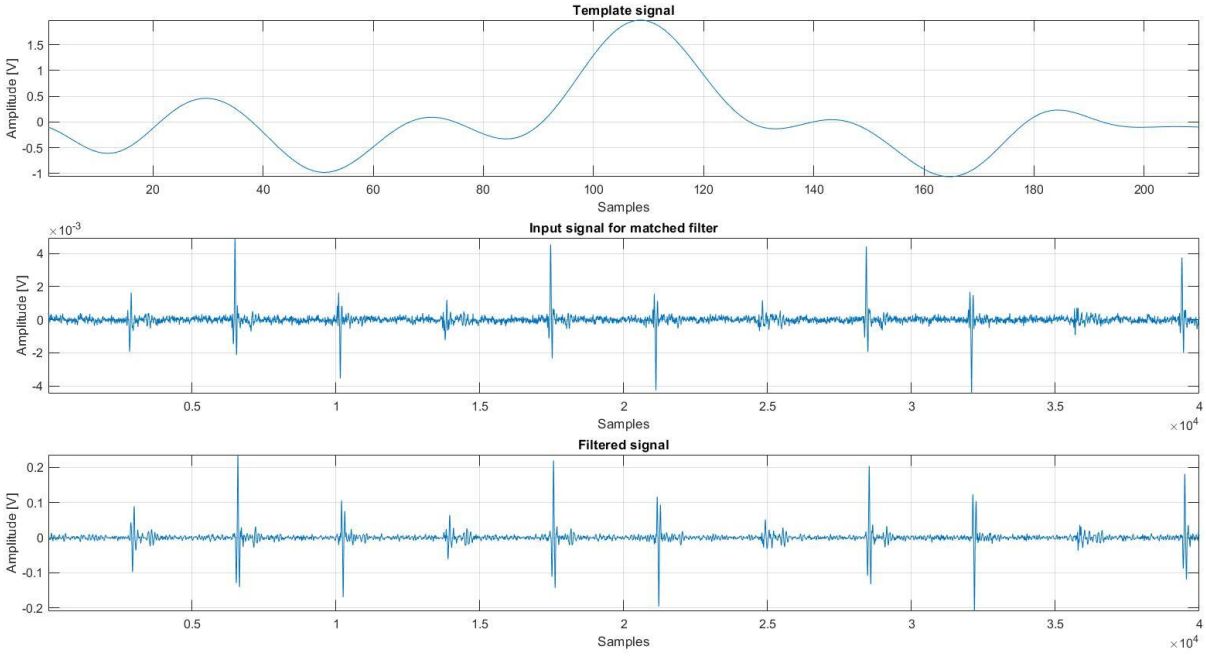


Figure 33. Template signal, input signal and the matched filter`s output

After applying the matched filter, the Search Subtract and Readjust algorithm was applied on a period of the signal to extract the multipath components. In the figure below, a period of the resulted signal in the time domain is presented:

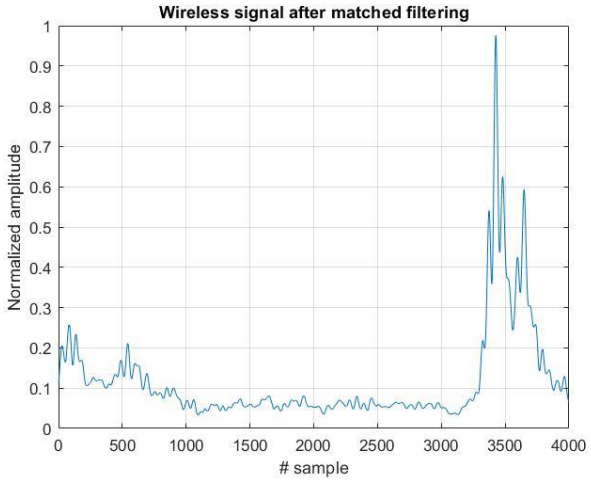


Figure 34. Wireless Signal after Matched Filter

SSR is based on the iterative correlation of the template waveform with the input signal and determines the set of amplitude and delay parameters, then extracting the template waveform with these parameters from the original signal.

The SSR method extracts the multipath components from the received signal and iteratively maximizes the signal to noise ratio and improves the time resolution in the signal, compared to Matched Filter, which maximizes the signal to noise ratio just once.

It is observed that there are three multipath components on a signal period, from which two are superposed, having a small-scale fading, due to the multipath propagation. Also, the strongest path is not always the first ray that arrives at the receiver and the later the rays arrive, the lower power they have. The time of arrival of the received signal is considered to be the moment when the first ray arrives at the receiver. Time of arrivals of the multipath components can be utilized in the positioning application, thus SSR could be an effective algorithm in this matter.

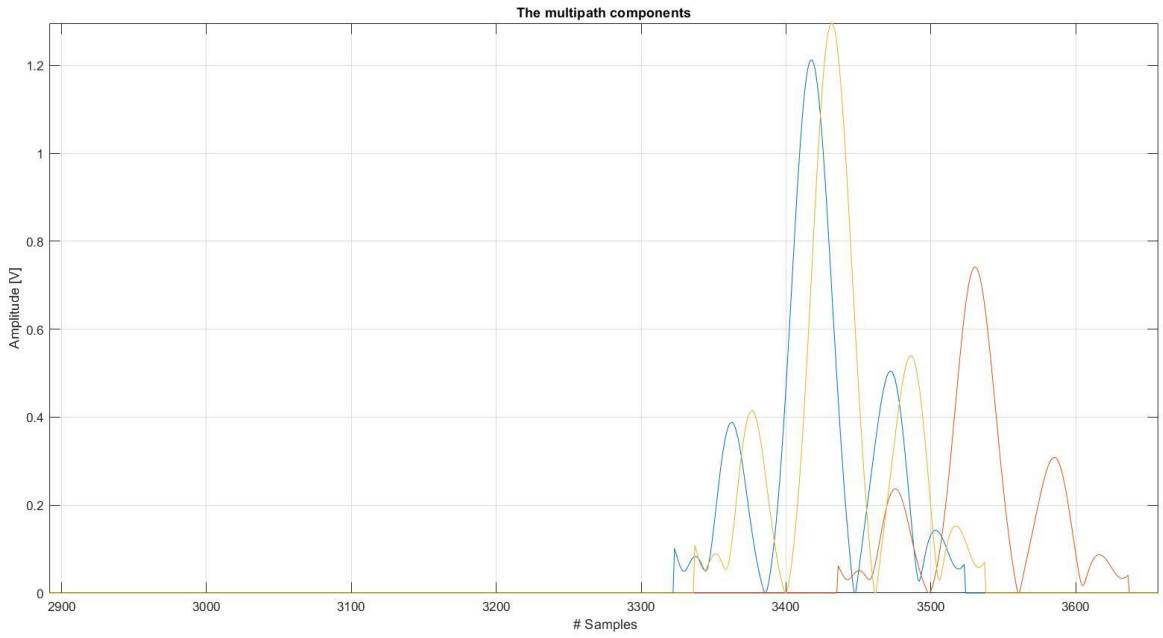


Figure 35 Wireless signal after SSR

## 4.2 Results and discussion for people detection and counting

By applying the algorithm for the hybrid features, frequency-based and time-based, on the dataset of radar samples, a set of 293 features are resulted. 280 features are extracted using the segmented-based feature extraction method, which include the energy and the maximum amplitude from the segmented signals and 13 features using the frequency-based method, which consist of the curvelet coefficients. The total feature vector for each radar sample of 50 received signals consists of 293 features, a smaller number of features than used in the reference paper.

The FDCT via wrapping method is applied to the preprocessed dataset of radar samples without clutter removal, to fully extract the statistical features. The data matrix is decomposed into three layers: fine, detail and coarse layer. The coarse layer contains the low-frequency coefficients and the fine layer contains the high-frequency coefficients.

Energy and the mean value are extracted as features from the coarse layer, which generally describe the data.

The finer edge information is described by the fine layer, from which the first 5 peaks of high-frequency coefficient values and the fine layer energy are extracted as features.

The detail layer contains coefficients corresponding to different directions in the trajectories of people. The coefficients are divided into 16 directions. According to the paper [18], the people who move away from the radar are represented by the coefficients in panels 1,16,8 and 9, in a $45^{\circ}$ direction. People who move towards the radar are represented by the $135^{\circ}$ direction, meaning the panels 4,5,12 and 13. The persons standing still in the radar range are represented by the coefficients on the $90^{\circ}$ directions, meaning the panels 6,7,14 and 15.

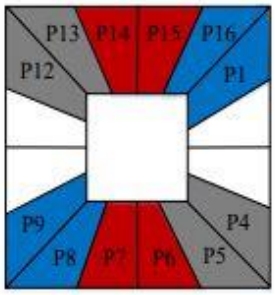


Figure 36. Index panel of directions from the detail layer [29]

The energy of the $90^{\circ}, 45^{\circ}, 135^{\circ}$ directions and high-frequency coefficients are extracted as features. The advantage of this feature extraction method is that more detailed features are provided, due to its anisotropic decomposition, providing detailed edge information.

The segmented-based features are extracted from each received signal of 1x1280 samples, thus for a radar sample of 50 x1280 values, the total vector of features will represent the mean of the extracted segmented-based feature extraction method features for each 1x1280 signal. For every received signal, 80 features concerning the energy and amplitude are extracted from the 32 length segment, 40 from the 64 length segment and 20 from the 128 length segment, both for band passed signals and for the signals without clutter. The advantage of this method is that it discriminates each person from the superposed signals, in a dense scenario, by choosing the length of each segment of 32, 64, or 128 samples, corresponding to physical parameters. Also, the segmented-based feature extraction method features are extracted from the band passed signals and the signals without noise and clutter, providing more detailed information.

The databased contains 6380 radar samples from which 293 features are extracted. The dataset was split in two parts: the training set and the test set. The training set was used for training the AI models, while the test set is used for model validation.

The results are given in the table below, in terms of accuracy, recall, f1-score, precision and cross-validation. We can observe that the greatest results are provided by Multilayer Perceptron Neural Network, followed by the K-nearest

neighbours algorithm. It is worth mentioning that KNN methods uses 5 neighbours, SVM uses the RBF kernel and MLP has 4 fully-connected layers of 50 neurons each.

Table 3. The classification performance for the 6380x293 set of features

| Algorithm | Accuracy | Precision | Recall | F1 score |
|---|---|---|---|---|
| K-NN | 94.08% | 94.08% | 94.08% | 94.00% |
| SVM | 85.12% | 85.12% | 85.12% | 82.76% |
| MLP | 99.85% | 99.85% | 99.85% | 99.85% |

The second approach is based on using a Convolutional Neural Network on the raw set of data. It is worth mentioning that the CNN was implemented using Pytorch, where a number of 100 000 parameters are constant updated, using 50 epochs (the iteration over the entire dataset). The purpose of the network is to minimize the error between the predicted data and the label, provided by a loss function, which is encoded using the one-hot encoding method. Based on the error, an optimizer is used to update the weights (the parameters). The optimizer used in the network is Adam optimizer, where the learning rate is adaptive. The loss function which is used is the Mean Squared Error which uses the L2 norm to compute the error between the predicted data and the target data.

The CNN is applied on the entire raw set of radar samples, and the results are provided in the Table 4.

Table 4. The performance of CNN for the set of raw data

| Algorithm | Accuracy | Precision | Recall | F1 score |
|---|---|---|---|---|
| CNN | 95.445 % | 95.445 % | 95.445 % | 95.445 % |

The architecture of the network is given in the figure below, whereas input it takes the radar sample of input 1x50x1280 samples:

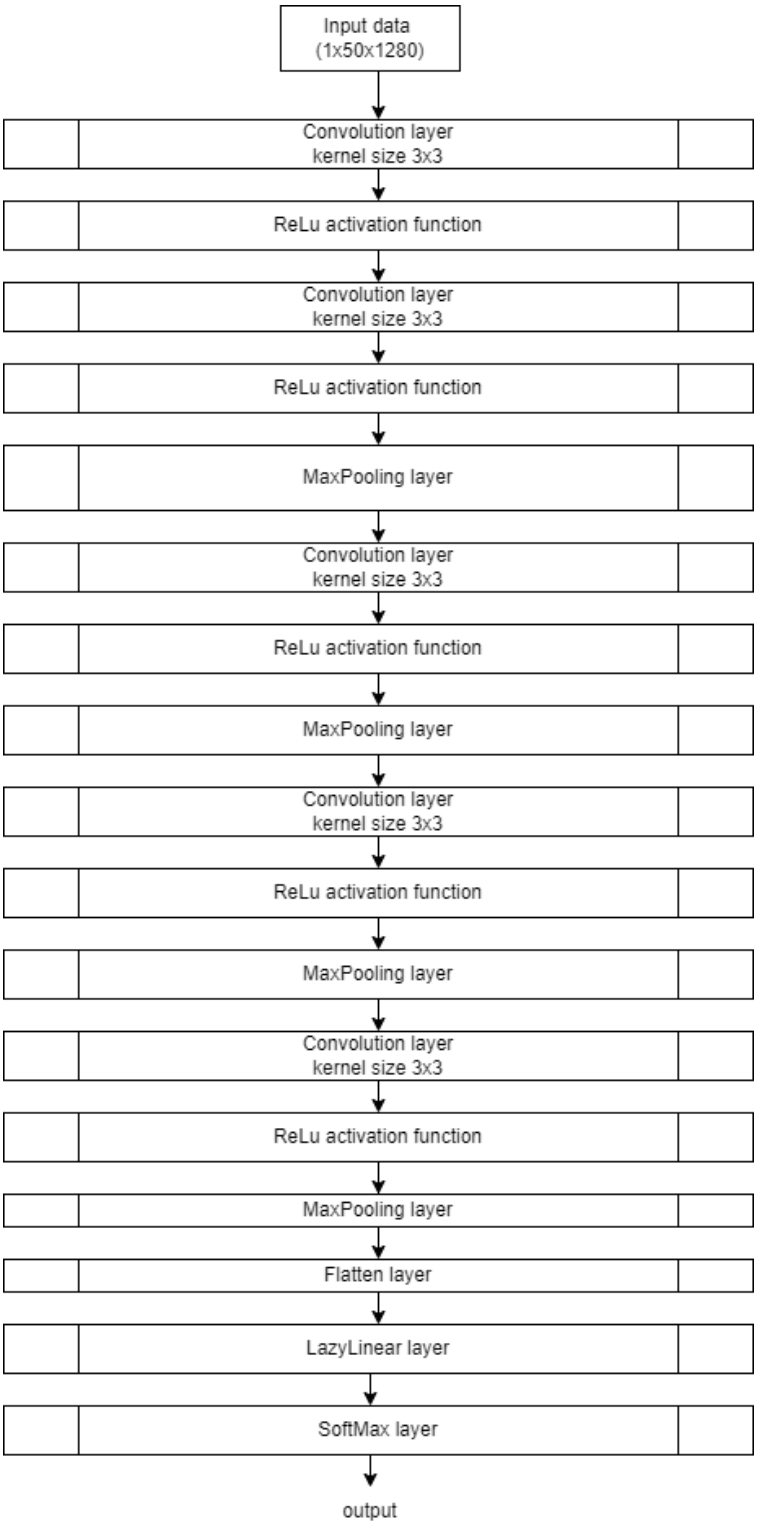


Figure 37. CNN architecture

80 din

The third approach proposes the Principal Component Analysis method for data compression, where the eigenvalues and eigenvectors of the covariance matrix of the dataset of 293 the already extracted hybrid features, are computed and sorted in descending order. A threshold of $0.95$ energy percentage of the largest selected eigenvalues of the data covariance matrix $C_Y$ is used to keep the most important principal components, to reduce the dimensions of the data.

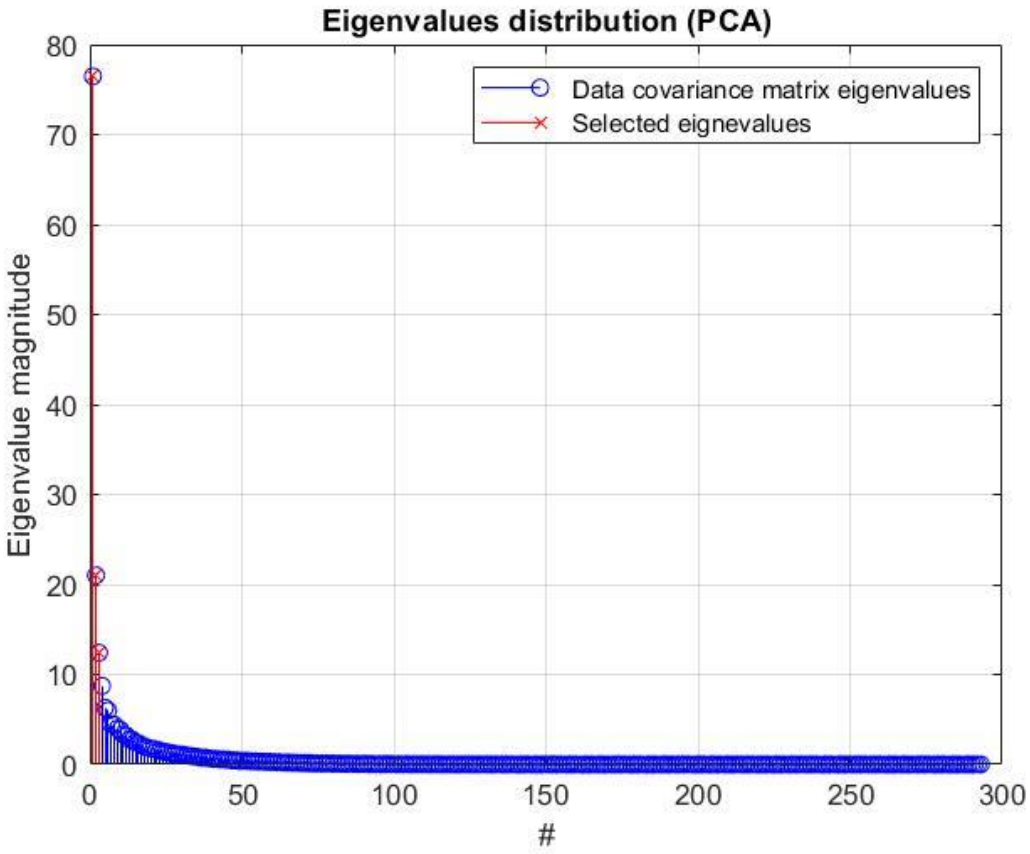


Figure 38. Eigenvalue distribution

By applying the threshold on the eigenvalues, only three of them are kept, corresponding to the three directions having the highest variance (amount of information), meaning that the new dataset has three dimensions in the projection space. The threshold influences the dimension of the new dataset and the loss of information.

The features extracted from the radar samples correspond to a fixed number of people in the radar range. PCA reduces the number of features, providing linear combinations of the initial ones, but the new variables correspond to the same specific number of persons in the radar range as the old features. For some random number of people, the data are visualized in three dimensions in the projection space, where $N_{num}$ represents the number of persons:

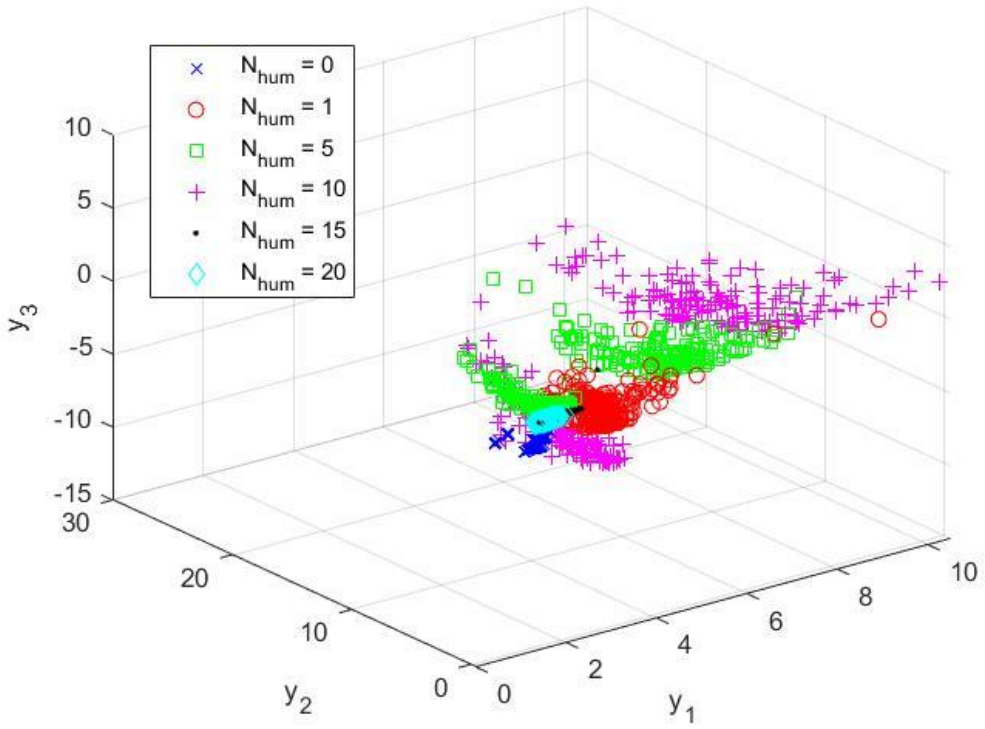


Figure 39 The projection space

The first principal component captures 36% of the information from the data matrix, while the second principal component captures 10% and the last 6% of the total energy (this percentage is given by the division of the corresponding eigenvalue to the sum of all eigenvalues).

The classification is done on the set of 6380x3 set of features, where the results are presented in table 5. We can observe that the highest performance is given by the K-nearest neighbours method, followed by MLP, which means that the architecture of MLP is not suitable for this dataset.

Table 5 The classification performance for the 6380x3 set of features

| Algorithm | Accuracy | Precision | Recall | F1 score |
|---|---|---|---|---|
| K-NN | 73.66% | 73.66% | 73.66% | 73.56% |
| SVM | 55.74% | 55.74% | 55.74% | 53.43% |
| MLP | 64.31% | 64.31% | 64.31% | 62.90% |

The PCA method is also applied on the entire set of data, where 6 principal components are extracted. CNN with only two layers of convolution is applied on the resulting dataset and the results are given in the table 6. It is worth mentioning that the network used almost 800 parameters to be updated, with the same hyper-parameters as the CNN applied on the entire raw set of data. The CNN architecture in this case is given as follows:

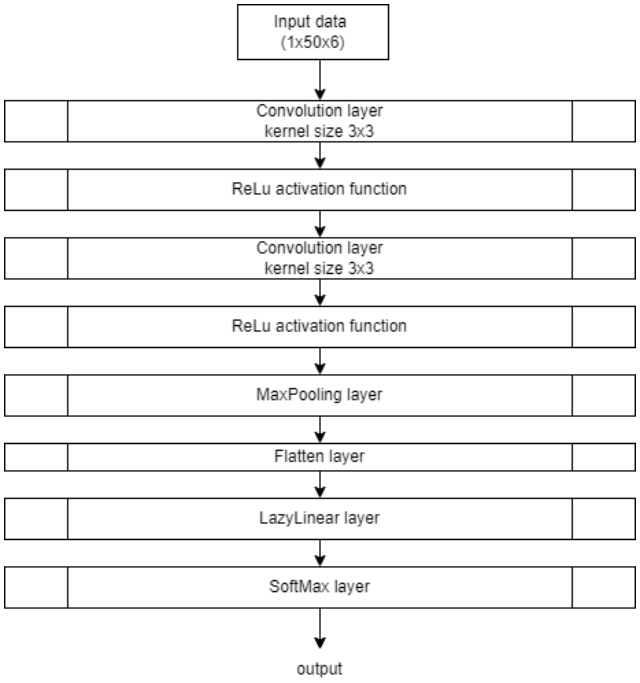


Figure 40. CNN architecture

Table 6 The performance of CNN for the set of PCA on the raw dataset

| Algorithm | Accuracy | Precision | Recall | F1 score |
|---|---|---|---|---|
| CNN | 95.41% | 95.41% | 95.41% | 95.41% |

## Conclusions

In conclusion, this paper presents some signal processing methods for ultra-wideband signals such as Envelope Detection using Hilbert Transform, Power Spectral Density Estimation via Welch's method, Baseband conversion, Matched Filter and Search Subtract and Readjust algorithm and an application for UWB signals, which is People Detection and Counting using an IR-UWB radar, based on Artificial Intelligence algorithms.

On the experimental signals, the signal's period is determined by using Envelope Detection using Hilbert Transform, the signal's bandwidth is determined by using Power Spectral Density Estimation via Welch's method, following by signal filtration, baseband conversion and multipath components extraction by using SSR algorithm. The SSR method extracts the multipath components from the received signal and iteratively maximizes the signal to noise ratio and improves the time resolution in the signal, compared to Matched Filter, which maximizes the signal to noise ratio just once. It is observed that there are three multipath components on a signal period, from which two are superposed, having a small-scale fading, due to the multipath propagation. Also, the strongest path is not always the first ray that arrives at the receiver and the later the rays arrive, the lower power they have.

The application proposed for UWB signals is People Detection and Counting using an IR-UWB radar, based on Artificial Intelligence algorithms, where the aim is to compare three approaches for feature extraction.

The three approaches refers to the set of features extracted from the database, which first proposes a complex algorithm composed of the Curvelet Transform and the Segmented-based feature extraction methods for frequency-based and time-based feature extraction, respectively, resulting in a set of 293 features. The second method proposes a Convolutional Neural Network for feature extraction and the third proposes the Principal Component Analysis method for data compression.

In real-time systems, the model provided by the CNN applied on the set of 6 components extracted by PCA is recommended, due to its effectiveness in terms of speed and computational demand. CNN applied on the entire set of data provides good results and it's more computationally expensive than the first method, where it requires the training of 100 000 parameters instead of 800 parameters as with the use of PCA. The algorithm used for extraction of the hybrid features provides great results, but it's not computationally effective and the complexity is higher. Data compression provided by PCA provides fast training and testing, but the data insufficiency can degrade the performance, if not a great dataset is used – the case of the dataset consisted of 3 features.

UWB technology is suitable for people detection and counting applications due to its fine temporal resolution and artificial intelligence algorithms provide high performance in terms of classification.

# Bibliography


[1] T. Kivinen, "datatracker.ietf.org," Internet Engineering Task Force (IETF), may 2017. [Online]. Available: https://datatracker.ietf.org/doc/html/rfc8137. [Accessed 15 06 2021].

[2] R. Yusnita, N. Razali, A. Tharek and H. P.S, "Ultra Wideband Technology and Its Applications," in *Wireless Communication Centre (WCC), Faculty of Electrical Engineering, Universiti Teknologi Malaysia 81310 Johor Bahru,Malaysia*, Department of Electronic, Electrical and Computer Engineering University of Birmingham Edgbaston Birmingham, B15 2TT United Kingdom.

[3] T. C. a. G. P. M. I. Marco Cavallaro, "Gaussian Pulse Generator for Millimeter-Wave," *IEEE TRANSACTIONS ON CIRCUITS AND SYSTEMS—I: REGULAR PAPERS, JUNE ,* Vols. NO. 6,VOL. 57, 2010.

[4] F. C. Commission, ""Revision of Part 15 of the Commission's Rules Regarding Ultra-Wideband Transmission Systems"," Fist Report and Order, ET Docket 98-153, FCC 02-48,April, 2002.

[5] I. Opperman, M. Hamalainen and J. Iinatti, UWB Theory and Applications, 2004.

[6] M. Andreas, "Ultra-Wide-Band Propagation Channels," in *Proceedings of IEEE*, 2009.

[7] A. Molisch, D. Cassioli, C.-C. Chong, S. Emami, A. Fort, B. Kannan, J. Karedak, J. Kunisch, H. Schantz, K. Siwiak and M. Win, "A Comprehensive Standardized Model for Ultrawideband Propagation Channels," *IEEE Transactions on Antennas and Propagation,* Vols. 54, no.11, 2006.

[8] V. C. Chen, F. Li, S.-S. Ho and H. Wechsler, "Micro-Doppler Effect in Radar: Phenomenon, Model and Simulation Study," *IEEE Transanctions on aerospace and electronic systems,* Vols. 42 , no. 1, 2006.

[9] J. Kwon, S. Lee and N. Kwak, "Human Detection by Deep Neural Networks Recognizing Micro-Doppler Signals of Radar," in *Proceedings of the 15th European Radar Conference* , 2018.

[10] V.-H. Nguyen and J.-Y. Pyun, "Location Detection and Tracking of Moving Targets by a 2D IR-UWB Radar System," *Sensors,* 2015.

[11] J.-H. Choi, J.-E. Kim and K.-T. Kim, "People Counting Using IR-UWB Radar Sensor in a Wide Area," *IEEE,* pp. 2327 - 4662, 2020.

[12] F. Diaconescu, "Impulse Radio UWB blind detectiong using Cross Recurrence Plot," in *2020 13th International Conference on Communications (COMM)*, Bucharest, Romania, 2020.

[13] S. Lim, J. Jung and S.-C. Kim, "Deep Neural Network-Based In-Vehicle People Localization Using Ultra-Wideband Radar," *IEEE ,* vol. 8, 2020.

[14] K. Youngwook and M. Taesup, "Human Detection and Activity Classification Based on Micro-Doppler Signatures Using Deep Convolutional Neural Networks," *IEEE GEOSCIENCE AND REMOTE SENSING LETTERS,* Vols. 13, NO. 1, January 2016.

[15] R. Qi, X. Li, Y. Zhang and Y. Li, "Multi-classification Algorithm for Human Motion Recognition Based on IR-UWB Radar," *IEEE Sensors Journal,* vol. 14, 2015.

[16] S. V. B. Joao, A. Zimmer and T. Brandmeier, "Pedestrian recognition using micro Doppler effects of radar signals based on machine learning and multi-objective optimization," *Expert Systems With Applications,* 2019.

[17] Y. Kim and H. Ling, "Human Activity Classification Based on Micro-Doppler Signatures Using a Support Vector Machine," *IEEE Transactions on Geoscience and Remote Sensing,* vol. 47, 2009.

[18] X. Yang, W. Yin, L. Li and L. Zhang, "Dense People Counting Using IR-UWB Radar with a Hybrid Feature Extraction Method," *IEEE Geoscience and Remote Sensing Letters,* vol. 16, no. 1, pp. 30-34, 2018.

[19] E. Candes , L. Demanet, D. Donoho and L. Ying, "Fast Discrete Curvelet Transforms," March 2006.

[20] M. Hozhabri, Human Detection and Tracking with UWB Radar, Stockholm: E-Print AB, 2019.

[21] C. SangHyun, M. Naoki and B. Joel, "An algorithm for UWB radar-based human detection," in *IEEE International Conference on Ultra-Wideband (ICUWB)*, Sydney, NSW, Australia doi:10.1109/ICUWB.2013.6663820, 2013.

[22] I. Oppermann, M. Hamalainen and J. Iinatti, UWB Theory and Applications, 2004.

[23] K. Yakup, W. Henk, M. Arjan, B. J. Mark and S. G. William, "An Experimental Study of UWB Device-Free Person Detection and Ranging," in *IEEE International Conference on Ultra-Wideband (ICUWB)*, Sydney, NSW, Australia doi:10.1109/ICUWB.2013.6663820, 2013.

[24] N. Van-Han and P. Jae-Young, "Location Detection and Tracking of Moving Targets by a 2D IR-UWB Radar System," *Sensors,* 2015.

[25] B. Schleicher and H. Schumacher, Impulse Generator Targeting the European UWB Mask, 2010.

[26] "A Summary of Worldwide Telecommunications Regulations governing the use of Ultra-Wideband radio," Decawave APPLICATION NOTE: APR001, 2015.

[27] I. Oppermann, M. Hamalainen and J. Iinatti, UWB Theory and Applications, 2004.

[28] L. Jing and Z. Zhaofa, "Through wall detection of human being's movement by UWB radar," in *The Society of Exploration Geophysicists to Chinese Geophysical Society*, Beijing, China, 2011.

[29] Q. Rui, L. Xiuping, Z. Yi and L. Yubing, "Multi-classification Algorithm for Human Recognition Based on IR-UWB Radar," *IEEE Sensors Journal,* Vols. 14, no. 8 , 2015.

[30] E. Anwar , S. Timothy, W. Safwan and X. Tian, "Machine Learning for Respiratory Detection Via UWB Radar Sensor".

[31] C. C. Victor , L. Fayin, H. Shen-Shyang and W. Harry, "Micro-Doppler Effect in Radar: Phenomenon, Model, and Simulation Study," *IEEE TRANSACTIONS ON AEROSPACE AND ELECTRONIC SYSTEMS,* Vols. 42,NO.1, 2006.

[32] A. Molisch, "Ultra-Wide-Band Propagation Channels," *Proceedings of the IEEE,* vol. 97, no. 2 DOI:10.1109/JPROC.2008.2008836, 2009.

[33] A. Molisch, "Ultra-Wide-Band Propagation Channels," in *Proceedings of the IEEE*, Vol.97 no. 2 2009.

[34] A. Molisch, D. Cassioli, C.-C. Chong, S. Emami, A. Fort, B. Kannan, J. Karedal, J. Kunisch, H. Schantz, K. Siwiak and M. Win, "A Comprehensive Standardized Model for Ultrawideband Propagation Channels," *IEEE Transactions on Antennas and Propagation,* vol. 54 no. 11, 2006.

[35] Z. Cui, Y. Gao, J. Hu, S. Tian and J. Cheng, "LOS/NLOS Identification for Indoor UWB Positioning Based on Morlet Wavelet Transform and Convolutional Neural Network," *IEEE Communications Letters,* 2020.

[36] F. Grejtak and A. Prokes, "UWB - ULTRA WIDEBAND CHARACTERISTICS AND THE SALEH-VALENZUELA," *Acta Electrotechnica et Informatica,* vol. 13 no. 2, p. 32–38, 2013.

[37] T. Ulrich, "Envelope Calculation from teh Hilbert Transform," March 2006.

[38] E.-T. Lee and H.-C. Eun, "Structural Damage Detection by Power Spectral Density Estimation Using Output-Only Measurement," *Hinwawi , Shock and Vibration,* 2016.

[39] J. C. Bancroft, "Introduction to matched filters," CREWES Research Rerport Volume 14, 2002.

[40] C. Falsi, D. Dardari, L. Mucchi and M. Win, "Time of Arrival Estimation for UWB Localizers in Realistic Environments," *EURASIP Journal on Applied Signal Processing,* vol. 2006, pp. 1-13.

[41] K. Jihoon, L. Seungeui and K. Nojun, "Human Detection by Deep Neural Networks Recognizing Micro-Doppler Signals of Radar," in *Proceedings of the 15th European Radar Conference*.

[42] D. Kocur, J. Gamec, M. Svecova, M. Gamcova and J. Rovnakova, "Imaginig Method: An efficient Algortihm for Moving Target Tracking by UWB Radar," *Acta Polytech.,* 2010.

[43] Z.-y. Zhang, X.-d. Zhang, H.-y. Yu and X.-h. Pan, "Noise suppression based on a fast discrete curvelet transform," *Journal of Geophysics and Engineering,* vol. 7, pp. 105-112, 2010.

[44] J. Fadili and J.-L. Starck, "Curvelets and Ridgelets," *R.A. Meyers, ed. Encyclopedia of Complexity and Systems Science ,* vol. 14, pp. 1718-1738, 2009.

[45] J. Ma and G. Plonka, "The Curvelet Transform," *IEEE Signal Processing Magazine,* 2010.

[46] Kassambara, "www.sthda.com," 23 09 2017. [Online]. Available: http://www.sthda.com/english/articles/31-principal-component-methods-in-r-practical-guide/112-pca-principal-component-analysis-essentials/. [Accessed 09 04 2021].

[47] Z. Jaadi, "https://builtin.com," 01 04 2021. [Online]. Available: https://builtin.com/data-science/step-step-explanation-principal-component-analysis. [Accessed 12 04 2021].

[48] "www.wikipedia.com," Wikipedia, 09 04 2021. [Online]. Available: https://en.wikipedia.org/wiki/Eigenvalues_and_eigenvectors. [Accessed 12 04 2021].

[49] S. Brunton and N. Kutz, Data-Driven Science and Engineering, Cambridge University Press,DOI: 10.1017/9781108380690, 2019.

[50] B. Schleicher and H. Schumacher , Impulse Generator Targeting the European UWB Mask, 2010.

[51] X. Guanlei, W. Xiaotong and X. Xiaogang, "Generalized Hilber transform and its properties in 2D LCT domain," *Signal Processing 89,* pp. 1395-1402, 2009.

[52] "www.wikipedia.com," 20 03 2021. [Online]. Available: https://en.wikipedia.org/wiki/Decision_tree. [Accessed 23 04 2021].

[53] B. Schleicher and H. Schumacher, Impulse Generator Targeting the European UWB Mask, 2010.

[54] F. Grejtak and A. Prokes, "UWB - ULTRA WIDEDBAND CHARACTERISTICS AND THE SALEH-VALENZUELA," *Acta Electrotehnica et Informatica,* vol. 13 . no. 2, pp. 32-38, 2013.